LUND UNIVERSITY

Quantum state tomography of attosecond electron wavepackets

Ron Demjaha
Supervisor: Anne L'Huillier
Assistant supervisor: Hugo Laurell

LRAP: 587

Contents

Abstract

In this master thesis, a broad theoretical description is done of a novel quantum state tomography protocol called KRAKEN. This protocol is meant for the determination of the density matrix of an electronic state created by absorption of XUV radiation in the vicinity of a Fano resonance. At first, a description of the KRAKEN protocol is provided. Then, the theory of Fano resonances is discussed. After that, the physics of two-photon transitions is presented. Finally, possible expansions of KRAKEN using chirped or broadband IR probe pulses, are examined.

1 Introduction

Quantum state tomography (QST) is a process by which one reconstructs the density matrix of a quantum system. This is analogous to the classical case, in which tomography means reconstructing a three-dimensional image of an object by measuring the two-dimensional cross-section many different times and piecing together these measruements into a three-dimensional image. Hopefully this image then approximates the original object in question. In the quantum mechanical case, each of these cross-sectional measurements then corresponds to a measurement in a certain basis, i.e. a projection of the object on the basis[1]. We have a ground state from which we have electronic transitions from photon absorption. We end up with an electron wavepacket in an energy continuum. By changing appropriate parameters for the photons, we can get the density matrix of the photoelectron, and we have a QST protocol.

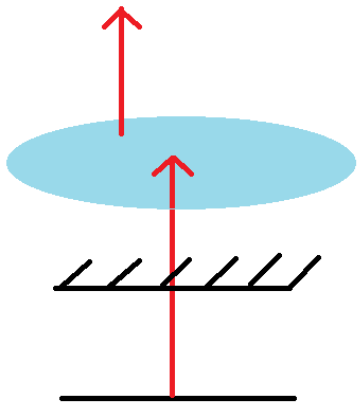

Figure 1: A schematic of the kind of transitions considered in this thesis. The red arrows correspond to electronic transitions due to photon absorption. The blue oval represents an electron wave packet in the continuum.

This thesis, then, aims to examine a new proposed method of quantum state

tomography called KRAKEN, which currently is only theoretically robust. This method is based on attosecond optics.

Previous measurements using attosecond pulses (for example RABBIT) have been used for the reconstruction of the *wave function* of the photoelectron (assuming perfect coherence).

This thesis will be separated into roughly four parts. The first part will focus on introducing the KRAKEN protocol and explain how it works. The case study for KRAKEN in our case will be the Fano resonances, which provide a specific instance of entanglement relevant to quantum optics. Essentially we apply the KRAKEN protocol to a photoelectron with an energy close to that of an autoionizing state. For these states, Fano resonances can occur[4]. After this, we need to perform an in-depth study on the physics of two-photon transitions, since KRAKEN is based on a two-photon transition pump-probe scheme (two photons since we have interaction with both an XUV and IR photon). This will be done perturbatively to the lowest necessary order, and the aim of this section will be to derive the transition amplitude of the transitions relevant to KRAKEN. Special care will be given to the two-photon transition matrix element, and a dipole approximation will be used to ground the theory in standard quantum optics.

Once the theoretical background and basic simulations have been presented, we will move on to potential expansions of KRAKEN that were examined over the course of this master thesis. Several topics were examined, but the two main ones are as follows: one is regarding the possibility of using a chirped pulse to significantly shorten the time of the KRAKEN measurements. The idea is straightforward: since KRAKEN QST requires us to use several (approximately) monochromatic pulses to perform all of the cross-sectional measurements required, one could for example use a chirped pulse to cover all of these frequencies within one single pulse. Essentially, having one pulse which is capable of scanning through all the frequencies necessary for performing quantum state tomography. Emphasis will be placed on how the presence of chirp affects the theory of the physics involved, essentially studying how the equations and derivations are affected by it. Simulation results with chirp added will be discussed as well.

The second possible expansion of KRAKEN that will be discussed is regarding the use of broadband radiation. The original protocol assumes monochromatic light, which of course is not consistent with experimental reality. The possibility of recovering the result for bichromatic fields, when using broadband radiation, is discussed. Again, emphasis was placed on the theoretical aspect of this data analysis, with some simulation results being included as a proof of concept, though the method needs to be further developed in order to actually be of use scientifically.

In summary, the aim of this thesis is primarily to serve as a theoretical description of KRAKEN and the theory required to understand it, coming from a range of papers from different research groups. Finally, some possible and original expansions of the protocol will be discussed.

2 KRAKEN protocol

Now, the KRAKEN protocol [2] will be described. At first, the general principles of the protocol will be discussed. Following this, a detailed derivation of the protocol (i.e. how the density matrix subdiagonals are acquired) will be presented. In order to understand why the KRAKEN protocol is being developed, consider the current state of attosecond interferometry. RABBIT and streaking are very good at recovering the wavefunctions of attosecond electron wavepackets. However, in order for this to fully characterize a quantum state, said state must be pure. If it is not, a full characterization requires the density matrix. This is what KRAKEN attempts to address, and so far the protocol in the original article [2] is purely theoretical. Some useful experimental data exists, however, and will be presented below.

First, as a reminder and to compare and contrast, consider RABBIT:

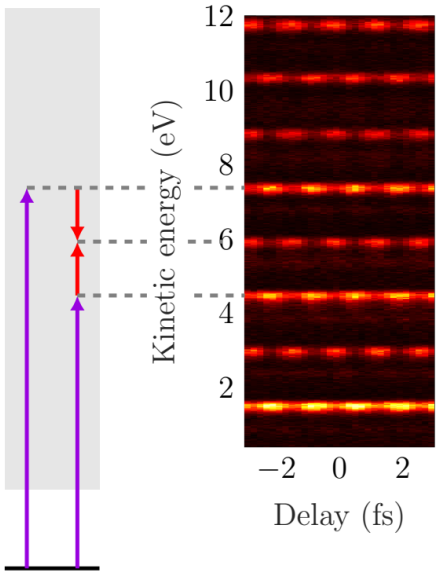

Figure 2: Energy levels of RABBIT to the left, where the two purple arrows correspond to adjacent harmonics, and the two red arrows correspond to an IR photon being absorbed and emitted, respectively. To the right is a scan with harmonics and sidebands. Figure taken from [3].

In RABBIT, and attosecond pulse train is generated through HHG (high order harmonic generation). In figure 2, the purple arrows denote two adjacent harmonics of the pulse train. There is also an IR field present. As can be seen in figure 2, if an IR photon is emitted and absorbed, respectively, by two adjacent harmonics we can reach the same energy through two quantum paths. This causes an interference phenomenon which can be seen as a beating

frequency in the sideband (to the right in the figure). The idea is that one can extract information on the phase and amplitude from the information in the scan, which allows the reconstruction of the wave function. As will be seen shortly, the interferometry of KRAKEN is very similar in principle but with some key differences.

2.1 General principles

The main idea behind KRAKEN is to perform quantum state tomography on electron wavepackets created by absorption of XUV pulses. In KRAKEN, an XUV pulse (i.e. a pulse generated through HHG) interacts with the target atom or molecule and ionizes it. Thus we have an EWP in the continuum. Furthermore, a bichromatic IR field is interacting with the system and as such couples different continuum states within the EWP bandwidth. The bandwidth of the EWP can be called $\delta\Omega$, and the bichromatic IR field has the frequencies ω_1 and ω_2. In the KRAKEN protocol, the electron spectrum is measured as a function of the time delay τ between the XUV pulse and the bichromatic IR field, as well as the frequency difference $\delta\omega = \omega_2$ - ω_1 between the two components of the IR field. One of the components, say ω_1 is fixed and kept close to $\delta\Omega$, while the other is varied from ω_1 to $\omega_1 + \delta\Omega/2$. This spectrum then, can be shown to be proportional to the subdiagonals of the ionized electron's density matrix.

The following schematic image illustrates the general physical situation at hand:

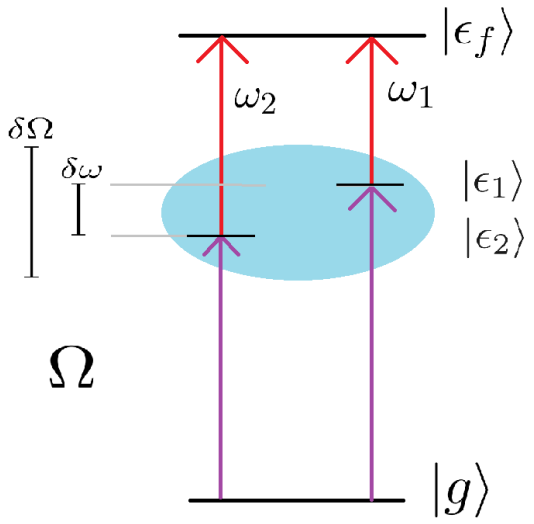

Figure 3: Energy diagram of transitions relevant to KRAKEN measurement. $|g\rangle$ is the ground state, Ω is the harmonic (which is also the purple arrows), the blue blob is the XUV electron wavepacket, $|\epsilon_1\rangle$ and $|epsilon_2\rangle$ are the IR probe energy levels and ω_1 and ω_2 are the energies of the two probes. $|\epsilon_f\rangle$ is the final energy. $\delta\omega$ is the shear frequency and $\delta\Omega$ is the XUV bandwidth.

Consider the energy levels in figure 3. While there is still a pulse train generated through HHG, much like in RABBIT, in this case the harmonics are broad. The two purple arrows in figure 3 are both from the same broad harmonic with central frequency Ω and bandwidth $\delta\Omega$. So the blue oval in the figure represents an EWP with different frequency components, due to the fact that the broad harmonic itself has different frequency components. Similarly to the RABBIT case, the interferometry is due to an IR field present, however in this case the field is bichromatic (i.e., there are two monochromatic components in the probe).

Now, consider the two energy levels $|\epsilon_1\rangle$ and $|\epsilon_2\rangle$ in the figure. The two IR probes are going to "hit" the EWP at different energies within the ionized gas, however what remains consistent is the energy difference $\delta\omega$ (which we call the shear frequency) between the two probe fields. As will be shown shortly, this is what is utilized to perform the KRAKEN measurement. Similarly to RABBIT, there are two quantum paths that lead to the same final energy, corresponding to the state $|\epsilon_f\rangle$ in figure 3. We expect this to lead to interference effects that we use for interferometry.

Now, consider what is actually measured when the above is perfomed. The scan that is acquired can be considered in analogy with the one for RABBIT

seen in figure 2:

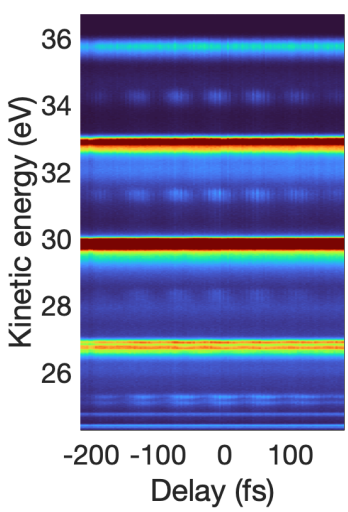

(a) KRAKEN scan, with probe delay in the horizontal axis and kinetic energy in the vertical axis. Note the broad harmonics and the faint sidebands.

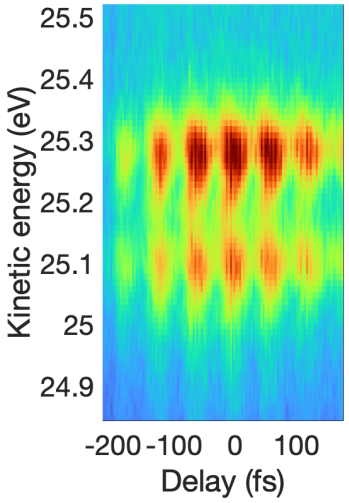

(b) Zoomed in version of image (a) showing a sideband.

Figure 4

To the left is the scan, which is from real experimental data. Similarly to RABBIT, we have the harmonics (note that they are broad in this case) and in between them we have the sidebands. The harmonics correspond to the broad XUV light pulses generated through HHG, while the sidebands are what we get from the interfering quantum paths leading to the state $|\epsilon_f\rangle$. Figure b) is a zoomed in image of one of the sidebands. It is there that we have the information used for KRAKEN. The beating frequency corresponds to the shear frequency $\delta\omega$, and as we will see it is the shear frequency we can change to extract all the information we need. The data in the scan, specifically the figure to the right, is a so-called electron spectrum, which we denote as $S(\varepsilon, \tau, \delta\omega)$.

The spectrum in question can be written as

$$S(\varepsilon, \tau, \delta\omega) = \langle \varepsilon | \, \rho_{\text{xuv+ir}} \, | \varepsilon \rangle \,,$$

where $\rho_{\text{xuv+ir}}$ is the continuous variable two-photon density matrix for the ejected electron. As will be shown below, the following holds:

$$S(\varepsilon,\tau,\delta\omega) \approx |\mu_{\varepsilon,\varepsilon_1}|^2 \langle\varepsilon_1|\rho_{\text{xuv}}|\varepsilon_1\rangle + |\mu_{\varepsilon,\varepsilon_2}|^2 \langle\varepsilon_2|\rho_{\text{xuv}}|\varepsilon_2\rangle + e^{i\delta\omega\tau}\mu_{\varepsilon,\varepsilon_1}\mu^*_{\varepsilon,\varepsilon_2}\langle\varepsilon_1|\rho_{\text{xuv}}|\varepsilon_2\rangle + e^{-i\delta\omega\tau}\mu_{\varepsilon,\varepsilon_2}\mu^*_{\varepsilon,\varepsilon_1}\langle\varepsilon_2|\rho_{\text{xuv}}|\varepsilon_1\rangle$$

where $\mu_{\varepsilon,\varepsilon_{1,2}}$ are the matrix elements for the dipole transitions and $\varepsilon_{1,2}$ = ε - $\omega_{1,2}$. Note that the first two terms in the spectrum as written above are populations and the remaining two are coherences. To acquire the density matrix subdiagonals, we simply want the coherences and to get these we take the Fourier transform over the spectrum with respect to the delay τ and then filter out the $\delta\omega$ component, which is the one we are after. This gives the subdiagonals as functions of the Fourier transform variable, which we can then have corresponding to the shear frequency $\delta\omega$, i.e. we vary this parameter to "scan" over all the different subdiagonals we are interested in. Put another way, we can choose the components oscillating at the frequencies $\pm\delta\omega$. This assumes that the dipole transition matrix elements are constant over the relevant energy range, so that we simply get that the Fourier transform is proportional to the subdiagonals and nothing else.

The density matrix in question is structured as seen in the figure below:

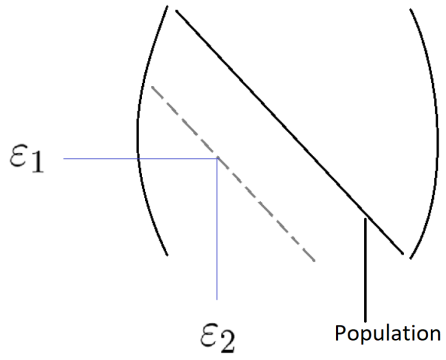

Figure 5: Structure of the matrix, as compared to the matrix elements derived from equation 2.1. The main diagonal contains the populations.

One parameter that is of particular interest here is the *purity*. Given a general density matrix ρ, the purity of the corresponding quantum system is defined as

$$\gamma \equiv \text{tr}(\rho^2).$$

One interpretation of the purity is that it tells us how much a state is mixed. If the purity is 1, it means that the state is pure as opposed to mixed. The purity is of interest since we can easily compare the theoretical purity of a given quantum system with the purity of the reconstructed density matrix. Thus, the purity is an indication of how good the protocol in question is. For example, the 2s2p resonance in helium theoretically corresponds to a pure state, and as such

one would expect the purity to be 1. For the KRAKEN simulation performed in the original paper [2], the purity of the reconstructed density matrix was found to be 0.96. This indicates that KRAKEN is quite robust in simulations. The error here was due to the small but finite bandwidth of the IR field employed (about 3 nm).

2.2 Detailed description of protocol

Here we describe a more detailed description of the KRAKEN protocol, which itself is an abbreviated version of the supplementary material to the original KRAKEN paper [2]. This treatment is based on the fact that the density matrix of the electron wave packet, following its interaction with the IR probe, is given by

$$\rho_{\mathrm{xuv+ir}} = U(\tau, \delta\omega)\rho_{\mathrm{xuv}}U^{\dagger}(\tau, \delta\omega)$$

where $U(\tau, \delta\omega)$ is a unitary matrix given by

$$U(\tau, \delta\omega) = \exp\left(-\frac{i}{\hbar}\int \mathrm{d}t\ \mathcal{H}_{\mathrm{ir}}(t)\right).$$

What we also need to establish is the Hamiltonian of the system, which is given by

$$\mathcal{H}_{\mathrm{ir}}(t) = -\frac{\hbar}{\sqrt{2\pi\sigma^2}}e^{-t^2/2\sigma^2}e^{-i(\omega-\omega_0)(t+\tau)}\left(\Pi_{\omega} + e^{-i\delta\omega(t+\tau)}\Pi_{\omega+\delta\omega}\right) + \mathrm{h.c.} \quad (1)$$

Here, Π_{ω} is the transition operator, which describes the transition driven by dipole radiation between the energy state $|\varepsilon\rangle$ to the energy $|\varepsilon+\omega\rangle$. We can write this operator as

$$\Pi_{\omega} = \int \mathrm{d}\varepsilon\ \mu_{\varepsilon+\omega,\varepsilon}\,|\varepsilon+\omega\rangle\langle\varepsilon|\,,$$

where in the above, μ denotes the dipole transition matrix elements such as $\mu_{\varepsilon+\omega,\varepsilon} = \langle\varepsilon+\omega|\,d\,|\varepsilon\rangle$. Here d is the dipole operator. Analogously, we also have

$$\Pi_{\omega+\delta\omega} = \int \mathrm{d}\varepsilon\ \mu_{\varepsilon+\omega+\delta\omega,\varepsilon}\,|\varepsilon+\omega+\delta\omega\rangle\langle\varepsilon|\,.$$

Inserting these into the integral expression for $U(\tau, \delta\omega)$ we arrive at the following:

$$\begin{aligned} U(\tau, \delta\omega) &= \exp\left(\frac{i}{\sqrt{2\pi\sigma^2}}\left(\int_{-\infty}^{\infty}\mathrm{d}t\ e^{-t^2/2\sigma^2}e^{-i(\omega-\omega_0)(t+\tau)}\left(\Pi_{\omega} + e^{-i\delta\omega(t+\tau)}\Pi_{\omega+\delta\omega}\right) + \mathrm{h.c.}\right)\right) \\ &= \exp\left(i\left(e^{-i(\omega-\omega_0)\tau}e^{-\frac{1}{2}(\omega-\omega_0)^2\sigma^2}\Pi_{\omega} + e^{-i(\omega+\delta\omega)\tau}e^{-\frac{1}{2}(\omega+\delta\omega)^2\sigma^2}\Pi_{\omega+\delta\omega} + \mathrm{h.c.}\right)\right) \quad . \end{aligned}$$

In order to simplify the remaining steps we introduce the following:

$$g_{\omega} = e^{-i(\omega-\omega_0)\tau}e^{-\frac{(\omega-\omega_0)^2\sigma^2}{2}}, \quad (2)$$

$$g_{\omega+\delta\omega} = e^{-i(\omega+\delta\omega)\tau} e^{-\frac{(\omega+\delta\omega)^2\sigma^2}{2}}, \tag{3}$$

$$\Pi = g_\omega \Pi_\omega + g_{\omega+\delta\omega}\Pi_{\omega+\delta\omega}. \tag{4}$$

Using the above, we can then write the unitary matrix $U(\tau, \delta\omega)$ as

$$U(\tau, \delta\omega) = \exp\left(i\left[\Pi + \Pi^\dagger\right]\right) \tag{5}$$

We can make the following approximation, since we have that the coupling constants g are small and satisfy $|g_\omega| \approx |g_{\omega+\delta\omega}| \equiv g_c$:

$$U(\tau, \delta\omega) \approx 1 + i\left[\Pi + \Pi^\dagger\right] + \mathcal{O}(g_c^2). \tag{6}$$

Now, what we want to do is consider the energy of the electron after interaction with both the pump and probe field. In order to do this, we take the following:

$$\begin{aligned}\langle\varepsilon|\,\rho_{\text{xuv+ir}}\,|\varepsilon\rangle &= \langle\varepsilon|\,U(\tau,\delta\omega)\rho_{\text{xuv}}U^\dagger(\tau,\delta\omega)\,|\varepsilon\rangle \\ &= \langle\varepsilon|\left(1 + i\left[\Pi + \Pi^\dagger\right] + \mathcal{O}(g_c^2)\right)\rho_{\text{xuv}}\left(1 - i\left[\Pi + \Pi^\dagger\right] + \mathcal{O}(g_c^2)\right).\end{aligned}$$

Doing the above, we get 9 terms, but some of them we can immediately see are zero. This is because we have that $\omega > \Delta\Omega$, where $\Delta\Omega$ is the spectral width of the XUV pulse. We then get

$$\langle\varepsilon|\,\Pi\rho_{\text{xuv}}\,|\varepsilon\rangle = \langle\varepsilon|\,\rho_{\text{xuv}}\Pi\,|\varepsilon\rangle = \langle\varepsilon|\,\Pi^\dagger\rho_{\text{xuv}}\,|\varepsilon\rangle = \langle\varepsilon|\,\rho_{\text{xuv}}\Pi^\dagger\,|\varepsilon\rangle = 0,$$

as well as

$$\langle\varepsilon|\,\Pi\rho_{\text{xuv}}\Pi\,|\varepsilon\rangle = \langle\varepsilon|\,\Pi^\dagger\rho_{\text{xuv}}\Pi^\dagger\,|\varepsilon\rangle = 0.$$

Thus, the expression for the energy becomes

$$\langle\varepsilon|\,\rho_{\text{xuv+ir}}\,|\varepsilon\rangle = \langle\varepsilon|\,\rho_{\text{xuv}}\,|\varepsilon\rangle + \langle\varepsilon|\,\Pi\rho_{\text{xuv}}\Pi^\dagger\,|\varepsilon\rangle + + \langle\varepsilon|\,\Pi^\dagger\rho_{\text{xuv}}\Pi\,|\varepsilon\rangle + \mathcal{O}(g_c^4). \tag{7}$$

We now end up with a large number of overlap integrals to compute, and all of these can be seen computed in the supplementary material to the KRAKEN paper. We will consider one of these, and because the rest will be very similar we will move directly to the final result and the way we treat it.

One of the overlap integrals we end up with is the following:

$$\begin{aligned}\langle\varepsilon|\,\Pi_\omega\rho_{\text{xuv}}\Pi_\omega^\dagger\,|\varepsilon\rangle &= \int \mathrm{d}\varepsilon'\mathrm{d}\varepsilon''\mu_{\varepsilon'+\omega,\varepsilon'}\mu^*_{\varepsilon''+\omega,\varepsilon''}\,\langle\varepsilon|\varepsilon'+\omega\rangle\,|\varepsilon'\rangle\,\rho_{\text{xuv}}\,|\varepsilon''\rangle\,\langle\varepsilon''+\omega|\varepsilon\rangle \\ &= |\mu_{\varepsilon,\varepsilon-\omega}|^2\,\langle\varepsilon-\omega|\,\rho_{\text{xuv}}\,|\varepsilon+\omega\rangle\,,\end{aligned}$$

and similarly for all the other overlaps. Doing this, we eventually end up

with the following:

$$\begin{aligned}
\langle\varepsilon|\,\rho_{\text{xuv+ir}}\,|\varepsilon\rangle = \langle\varepsilon|\,\rho_{\text{xuv}}\,|\varepsilon\rangle \\
&+ |g_\omega|^2|\mu_{\varepsilon,\varepsilon-\omega}|^2\,\langle\varepsilon-\omega|\,\rho_{\text{xuv}}\,|\varepsilon-\omega\rangle \\
&g_\omega g^*_{\omega+\delta\omega}\mu_{\varepsilon,\varepsilon-\omega}\mu^*_{\varepsilon,\varepsilon-\omega-\delta\omega}\,\langle\varepsilon-\omega|\,\rho_{\text{xuv}}\,|\varepsilon-\omega-\delta\omega\rangle \\
&g_{\omega+\delta\omega}g^*_{\omega}\mu_{\varepsilon,\varepsilon-\omega-\delta\omega}\mu^*_{\varepsilon,\varepsilon-\omega}\,\langle\varepsilon-\omega-\delta\omega|\,\rho_{\text{xuv}}\,|\varepsilon-\omega\rangle \\
&+ |g_{\omega+\delta\omega}|^2|\mu_{\varepsilon,\varepsilon-\omega-\delta\omega}|^2\,\langle\varepsilon-\omega-\delta\omega|\,\rho_{\text{xuv}}\,|\varepsilon-\omega-\delta\omega\rangle \\
&g^*_{\omega}g_{\omega+\delta\omega}\mu^*_{\varepsilon,\varepsilon+\omega}\mu_{\varepsilon,\varepsilon+\omega+\delta\omega}\,\langle\varepsilon+\omega|\,\rho_{\text{xuv}}\,|\varepsilon+\omega+\delta\omega\rangle \\
&g_\omega g^*_{\omega+\delta\omega}\mu_{\varepsilon,\varepsilon+\omega}\mu^*_{\varepsilon,\varepsilon+\omega+\delta\omega}\,\langle\varepsilon+\omega+\delta\omega|\,\rho_{\text{xuv}}\,|\varepsilon+\omega\rangle \\
&+ |g_{\omega+\delta\omega}|^2|\mu_{\varepsilon,\varepsilon+\omega+\delta\omega}|^2\,\langle\varepsilon+\omega+\delta\omega|\,\rho_{\text{xuv}}\,|\varepsilon+\omega+\delta\omega\rangle \\
&+ \mathcal{O}(g_c^4).
\end{aligned}$$

Since the above expression is a population we know we can measure it experimentally (it is in fact an energy expectation value). What we want to do is take a Fourier transform of this data such that it depends on the shear frequency $\delta\omega$. If this gives us the subdiagonals of the density matrix of the photoelectron, we know that we have a protocol for quantum state tomography. We introduce the following to simplify the expression:

$$g_\omega = h_\omega e^{-i(\omega-\omega_0)\tau} \equiv e^{-i(\omega-\omega_0)\tau}e^{-\frac{1}{2}(\omega-\omega_0)^2\tau^2}$$

Doing this, it can be shown that we get

$$\begin{aligned}
S_{\mathcal{F}} = &g_\omega g^*_{\omega+\delta\omega}\mu_{\varepsilon,\varepsilon-\omega}\mu^*_{\varepsilon,\varepsilon-\omega-\delta\omega}\,\langle\varepsilon-\omega|\,\rho_{\text{xuv}}\,|\varepsilon-\omega-\delta\omega\rangle \\
&+ g_\omega g^*_{\omega+\delta\omega}\mu_{\varepsilon,\varepsilon+\omega}\mu^*_{\varepsilon,\varepsilon+\omega+\delta\omega}\,\langle\varepsilon+\omega+\delta\omega|\,\rho_{\text{xuv}}\,|\varepsilon+\omega\rangle
\end{aligned}$$

We thus get two components, and can choose to filter out one of them so we are left with the final result:

$$S_{\mathcal{F}} = g_\omega g^*_{\omega+\delta\omega}\mu_{\varepsilon,\varepsilon-\omega}\mu^*_{\varepsilon,\varepsilon-\omega-\delta\omega}\,\langle\varepsilon-\omega|\,\rho_{\text{xuv}}\,|\varepsilon-\omega-\delta\omega\rangle$$

Thus, if we take this measurement for different $\delta\omega$, we can reconstruct the density matrix ρ_{xuv} to good approximation. This protocol thus is a theoretically valid quantum state tomography.

2.3 Case study

Now that the general principles of KRAKEN have been laid out, the next question to consider is what EWP we should study. There are two general criteria to consider here, we want a wave packet with *structure*, so that there is something to actually study that we understand well. And we also want a wave packet that exhibits *entanglement*, to necessitate the use of QST to fully characterize it. In our case, the structure will come from Fano resonances and the entanglement will come from *spin-orbit interactions*. More specifically, the transition to

be considered which exhibits these properties will be the $3s^{-1}4p$ transition in argon.

Aside from that, another transition that will be studied (and contrasted with that of argon) is the $2s2p$ transition in helium, which is a pure state as will be seen shortly.

In the following sections, the Fano resonances and the effects of spin-orbit interactions will be discussed in more detail. After that, the density matrix for said argon EWP will be shown and discussed.

3 Fano resonances

The Fano resonance is a physical phenomenon that shows up in many areas of physics (for example atomic physics, nuclear physics, optics, condensed matter physics, engineering applications in electrical circuits, microwave engineering, some materials science and so on) and has a wide variety of applications. For this master thesis, the Fano resonances will show up in a manner very close to how they were originally discussed, namely during electron transitions within atomic systems due to interaction with dipole electric fields. It is central to this thesis, since the transitions studied will be subject to said resonances. The resonance phenomenon was originally studied because the absorption cross-section of photons on a target atom exhibited asymmetries which were not properly explained by the quantum physics at the time. As such, Fano presented in his paper a rigorous mathematical description of how this asymmetry came to be. In this section, we will begin by recollecting the important parts of this derivation to lay the mathematical foundation for understanding the Fano profile. Said profile will then be discussed in more detail. Once that is done, we will conclude by considering the phase properties of the Fano transitions. The most important aspect of this final discussion is the expression for the transition amplitudes, which will be central to the next section where we derive the transition amplitudes used in the simulations of the KRAKEN protocol.

3.1 Theory of Fano resonances

Fano resonances occur because electrons changing energy levels in atoms can access both bound states and continuum states. This interaction causes an interference effect.

3.1.1 One bound state and one continuum

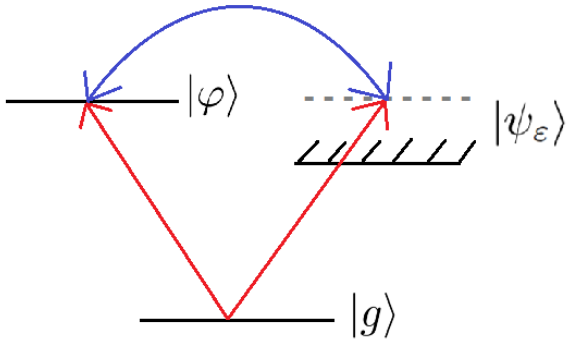

Figure 6: Energy diagram showing the transitions. We have a ground state $|g\rangle$, and the red arrows show the two paths we can go during transition. We have the bound state $|\varphi\rangle$ and a set of continuum states $|\psi_\varepsilon\rangle$. The blue double-ended arrow denotes the Fano resonance between the states.

As can be seen in figure 6, we have a discrete bound state $|\varphi\rangle$ and a set of continuum states we denote by $|\psi_\varepsilon\rangle$. When we have a transition from the ground state $|g\rangle$, we get an interference between the bound state and the continuum states (different possible pathways for the electron will be superposed with each other, as is typical of quantum physics). The photoelectron, i.e. the electron excited by light such that it transitions as described in the energy diagram, can then be represented as an electronic state that is a superposition of the possible states it can end up in, as follows:

$$|\Psi_E\rangle = a\,|\varphi\rangle + \int \mathrm{d}\varepsilon\; b_\varepsilon\,|\psi_\varepsilon\rangle \tag{8}$$

with the two terms corresponding to the aforementioned different sets, where $|\varphi\rangle$ are bound states and $|\psi_\varepsilon\rangle$ are continuum states. The coefficients a and b_ε are functions of E and are to be determined in order for us to understand how Fano resonances work. In order to do this we need to consider the following transition matrix elements [4]:

$$\begin{aligned}
\langle\varphi|\,H\,|\varphi\rangle &= E_\varphi,\\
\langle\psi_\varepsilon|\,H\,|\varphi\rangle &= V_\varepsilon,\\
\langle\psi_{\varepsilon'}|\,H\,|\psi_\varepsilon\rangle &= \varepsilon\delta(\varepsilon'-\varepsilon).
\end{aligned}$$

Here H is the hamiltonian of the system. What we want to do now is consider the time-independent Schrödinger equation,

$$H\,|\Psi_E\rangle = E\,|\Psi_E\rangle\,. \tag{9}$$

Taking the Schrödinger equation and multiplying by $\langle\varphi|$ and $\langle\psi_\varepsilon|$ from the left, respectively, we end up with the system of equations from which we can get the coefficients we are interested in:

$$E_\varphi a + \int \mathrm{d}\varepsilon \; b_\varepsilon V_\varepsilon^* = Ea, \tag{10}$$

$$V_\varepsilon a + \varepsilon b_\varepsilon = E b_\varepsilon. \tag{11}$$

Solving the above system of equations requires quite a bit of algebra, as well as the assumption that the electrons behave as plane waves when they are far enough removed from the atomic nucleus. The most important steps will be outlined here, as well as where the physical assumptions become relevant.

The first thing we do is that we try to express b_ε in terms of a, i.e. simply get rid of one of the two unknowns. If one considers equation 11, we see that we can rewrite it as follows:

$$b_\varepsilon = \frac{V_\varepsilon a}{E - \varepsilon}. \tag{12}$$

However, the expression in equation 12 has a pole for some of the energy values we might expect to get in a physical scenario. As such, we need to employ a trick to get around this issue. We introduce the following solution, which was formalized by Dirac:

$$b_\varepsilon = \left[\frac{1}{E-\varepsilon} + z(E)\delta(E-\varepsilon)\right] V_\varepsilon a. \tag{13}$$

To be more specific, the trick is to consider quantization in a finite box, so that one ends up working with a discrete spectrum as opposed to a continuous one. This case can then be considered for the limit case of an infinite box. The procedure will not be outlined in detail here though, and the reader is advised to take the above result as given. What $z(E)$ actually is will be discussed shortly.

Now we consider how to proceed with equation 13. What we note is that when integration is taken over the term with the pole, we take the principal value of the integral. What we then do is consider the approximation that the ejected electron is a plane wave.

$$\psi_\varepsilon \propto \sin(k(\varepsilon)r + \delta), \tag{14}$$

where δ is some phase. The reason this approximation is valid is that we assume we are far away from the atomic nucleus when the electron is in the continuum, which is a standard approximation in this type of atomic physics. With this form for ψ_ε, we then consider what happens with the integral in equation 8. We get in the integral two terms, which will be the sine expression multiplied by our expression for b_ε. The first term will be the integral taken over the product of the sine function and the term $(E-\varepsilon)^{-1}$, and using contour integration, one can show that the contribution from this first term is $-\pi\cos(k(E)r+\delta)V_E a$ for sufficiently large r, and similarly for the second term we get $z(E)\sin(k(E)r+\delta)V_E a$. What this means is that we can write the following for the sum of the two terms, using elementary trigonometry:

$$\int \mathrm{d}_\varepsilon \psi_\varepsilon \propto \sin(k(E)r + \delta + \Delta) V_E a, \tag{15}$$

where we now also have the term $\Delta = -\arctan(\pi/z(E))$ which corresponds to the phase shift we get due to the interaction between the ψ_ε and the φ states.

Now that we have an approximation for ψ_ε (making it a known variable, essentially) as well as having used equation 8, we can also determine $z(E)$ by substituting the expression for b_ε (in equation 13) in equation 10. Note that if we do this, we get the coefficient a on all terms, so we get rid of it and what remains is

$$E_\varphi + F(E) + z(E)|V_E|^2 = E, \tag{16}$$

where

$$F(E) = P \int \mathrm{d}\varepsilon \frac{|V_\varepsilon|^2}{E - \varepsilon}, \tag{17}$$

where P denotes the principal value of the integral. $z(E)$ can then immediately be recovered from equation 16:

$$z(E) = \frac{E - E_\varphi - F(E)}{|V_E|^2}. \tag{18}$$

Now, we have enough information to determine a to a satisfactory degree. In order to actually compute this we need to use a normalization condition $\left\langle \Psi_{\overline{E}} \middle| \Psi_E \right\rangle = \delta(\overline{E} - E)$:

$$\left\langle \Psi_{\overline{E}} \middle| \Psi_E \right\rangle = a^*(\overline{E}) a(E) + \int \mathrm{d}\varepsilon b_\varepsilon^*(\overline{E}) b_\varepsilon(E) = \delta(\overline{E} - E). \tag{19}$$

Since we have already expressed b_ε in terms of a in equation 13, and we have already arrived at an expression for $z(E)$, we can substitute the expression for b_ε into the above expression and use that to solve for a. This part is pure algebra, with the exception of the following result one can use to perform the computations [4]:

$$\begin{aligned} \frac{1}{(\overline{E} - \varepsilon)(E - \varepsilon)} &= \frac{1}{\overline{E} - E} \left(\frac{1}{E - \varepsilon} - \frac{1}{\overline{E} - \varepsilon} \right) \\ &+ \pi^2 \delta(\overline{E} - E) \delta(\varepsilon - \frac{1}{2}(\overline{E} + E)). \end{aligned}$$

Considering the above, we end up with

$$\begin{aligned} &|a(E)|^2 |V_E|^2 (\pi^2 + z^2(E)) \delta(\overline{E} - E) + a^*(\overline{E}) \\ &\times \left(1 + \frac{1}{\overline{E} - E} (F(E) - F(\overline{E}) + z(E)|V_E|^2 - z(\overline{E})|V_{\overline{E}}|^2) \right) a(E) = \delta(\overline{E} - E). \end{aligned}$$

Now, we can finally arrive at an expression for a. The above expression can be simplified by considering the relation $F(E) = -E_\varphi - z(E)|V_E|^2 + E$ that we

derived above, and the analogous relation for $F(\overline{E})$. Namely, the fact that we have

$$\begin{aligned} F(E) - F(\overline{E}) + z(E)|V_E|^2 - z(\overline{E})|V_{\overline{E}}|^2 \\ = -E_\varphi - z(E)|V_E|^2 + E + E_\varphi + z(\overline{E})|V_{\overline{E}}|^2 - \overline{E} + z(E)|V_E|^2 - z(\overline{E})|V_{\overline{E}}|^2 \\ = E - \overline{E}. \end{aligned}$$

Insert this relation into the brackets of the expression we derived earlier, we can see that the expression inside the brackets disappears and we are left with

$$|a(E)|^2 = \frac{1}{|V_E|^2(\pi^2 + z^2(E))} \tag{20}$$

We can get a more useful expression for a than the one above, and in fact we find that a oscillates as a function of the energy. In order to show this, one can consider the fact that we have the following

$$a(E) = \frac{1}{\pi V_E} \frac{1}{\sqrt{1 + (z(E)/\pi)^2}} \tag{21}$$

We can therefore write a as a sinusoidal function of Δ using the following arguments: we know from before that we have $\Delta = -\arctan(\pi/z(\mathrm{E}))$, which means that we can write $\pi/z(E) = \tan(-\Delta) = y/x$ for some trigonometrically relevant y and x on the unit circle. This means that we have

$$\begin{aligned} \sin(\Delta) = \frac{y}{\sqrt{x^2 + y^2}} = \frac{1}{\sqrt{1 + (x/y)^2}} = \frac{1}{\sqrt{1 + (-x/y)^2}} \\ = \frac{1}{\sqrt{1 + 1/\tan^2(-\Delta)}} = \frac{1}{\sqrt{1 + (z(E)/\pi)^2}}, \end{aligned}$$

which means that we can rewrite our expression for $a(E)$ as

$$a(E) = \frac{1}{\pi V_E} \frac{1}{\sqrt{1 + (z(E)/\pi)^2}} = \frac{\sin(\Delta)}{\pi V_E}, \tag{22}$$

which is our final expression for the coefficient a. Using this, we can then arrive at a similar expression for our coefficients b_ε. Performing this algebra, one can arrive at an expression for b_ε that also oscillates with respect to Δ. The results for the two coefficients are collected below, and are the main result of this rather lengthy mathematical derivation:

$$a = \frac{\sin\Delta}{\pi V_E}, \tag{23}$$

$$b_\varepsilon = \frac{V_\varepsilon}{\pi V_E^*} \left[\frac{\sin\Delta}{E - \varepsilon} - \pi \cos(\Delta) \delta(E - \varepsilon) \right], \tag{24}$$

as well as

$$z(E) = -\pi \cot\Delta. \tag{25}$$

From this we can then get the Fano profile. In order to proceed with our mathematical treatment, we must first understand what is interesting about what we have arrived at. Of course, the results in equations 23 and 24 allows us to describe the eigenvector Ψ_E, but the point of deriving the equations on this particular form (i.e. oscillations of Δ) is that what we are really interested in is the variation in the probability of excitation of the stationary state Ψ_E. In order to formalize this further, we want to introduce a transition operator T describing the transition from an initial state $|i\rangle$ and the final state $|\Psi_E\rangle$. Using the form of the final state we see in equation 8 in combination with the expressions seen in equations 23 and 24 we get the following matrix element representation for the transition operator:

$$\begin{aligned}\langle\Psi_E|\,T\,|i\rangle &= \frac{1}{\pi V_E^*}\,\langle\varphi|\,T\,|i\rangle\sin\Delta \\ &\quad + \frac{1}{\pi V_E^*}P\int \mathrm{d}\varepsilon\frac{V_\varepsilon^*\,\langle\psi_\varepsilon|\,T\,|i\rangle}{E-\varepsilon}\sin\Delta - \langle\psi_E|\,T\,|i\rangle\cos\Delta \\ &= \frac{1}{\pi V_E^*}\,\langle\phi|\,T\,|i\rangle\sin\Delta - \langle\psi_E|\,T\,|i\rangle\cos\Delta\end{aligned}$$

where we introduced ϕ as simply being the following combination of states:

$$|\phi\rangle = |\varphi\rangle + P\int \mathrm{d}\varepsilon\frac{V_\varepsilon\,|\psi_\varepsilon\rangle}{E-\varepsilon}. \tag{26}$$

Now that we have arrived here we are ready to discuss the famed Fano profile, which is the goal of this section of the thesis. What we want to consider is the following ratio:

$$\frac{|\,\langle\Psi_E|\,T\,|i\rangle\,|^2}{|\,\langle\psi_E|\,T\,|i\rangle\,|^2}. \tag{27}$$

Note that we have Ψ_E in the numerator and ψ_E in the denominator. If one takes a look at the expression for Δ, it can be seen that it varies extremely sharply as the variable E passes through the resonance at $E = E_\varphi + F$. This behaviour will, in turn, cause a very sharp variation of the transition matrix element $\langle\Psi_E|\,T\,|i\rangle$. That is to say, we expect some interesting sharp behaviour for the transition probability from our initial to final state as we approach this resonance. If one examines the above expression even closer, one can note that $\sin\Delta$ is an odd function of Δ and $\cos\Delta$ is an even function of Δ. As such, we have two terms $\langle\phi|\,T\,|i\rangle$ and $\langle\psi_E|\,T\,|i\rangle$ that interfere with each other with opposite phase. This interference is consistent with what we outline previously, where the physical interpretation is that we have continuum and bound states that interfere when we consider an electron being taken from its ground state by absorption of a photon (represented by the transition operator T). Note that ϕ has an extra integral term with it, which corresponds to the bound states being *modified* by the fact that V_ε and ψ_ε are both dependent on ε (there are theoretical treatments in some papers where this is not the case and in those instances the integral term vanishes and we are left with just the original bound state).

One thing that is interesting about expression 27 is that the numerator is proportional to the absorption cross section for a photon. What we can now use is that expression 27 can be parametrized as

$$\frac{|\langle\Psi_E|T|i\rangle|^2}{|\langle\psi_E|T|i\rangle|^2} = \frac{(q+\epsilon)^2}{1+\epsilon^2} = 1 + \frac{q^2-1+2q\epsilon}{1+\epsilon^2}, \tag{28}$$

where

$$q = \frac{\langle\phi|T|i\rangle}{\pi V_E^* \langle\psi_E|T|i\rangle}. \tag{29}$$

and ϵ here is the so-called reduced energy variable

$$\epsilon = -\cot\Delta = \frac{E - E_\varphi - F(E)}{\pi|V_E|^2} = \frac{E - E_\varphi - F}{\Gamma/2}. \tag{30}$$

Note that ϵ here is not the same as ε. The latter is the continuum variable, and not the reduced energy. This distinction is notationally subtle but will be crucial for understanding the later parts of this thesis. For the energy variable above, we have that $\Gamma = 2\pi|V_E|^2$ corresponds to the spectral width of the autoionized state φ. More specifically this is the spectral width of the resonance. One can plot this ratio, then, for different values of q, and this is what is discussed below while anchored in a less abstract and more physical interpretation than the one outlined above.

Now, we want to consider the special case where the transition operator T is, specifically, that of a dipole transition. For this case, we can call it $\mathcal{O}$, where $\mathcal{O} = \vec{\mathcal{O}} \cdot \hat{\epsilon}$, where $\vec{\mathcal{O}}$ is the dipole operator and $\hat{\epsilon}$ is the polarization direction of the light in question. Using the above result, we immediately find

$$\langle\Psi_E|\mathcal{O}|i\rangle = \frac{q+\epsilon}{\epsilon - i}\langle\psi_E|\mathcal{O}|i\rangle \tag{31}$$

which is important for this thesis, since it expresses the dipole transition from the first state $|i\rangle$ to the final state $|\Psi_E\rangle$ for the case where the final state is subject to a Fano resonance. We thus have, on the right-hand side of equation 31, the transition to the continuum but modified by the Fano resonance. This expression will be used later when constructing the theory for the simulations.

Taking the absolute square of the above transition matrix element, we get something that is proportional to a cross-section of the absorption, as follows:

$$\sigma(E) = \sigma_{bg}(E)\frac{(\epsilon + q_{\tilde{a}g})^2}{\epsilon^2 + 1} \tag{32}$$

where σ_{bg} is the background cross-section, which corresponds to direct photoionization. This cross-section is then multiplied by the Fano profile. Note that in the limit of ε going to infinity we get only the background cross-section since the Fano profile factor is unity. This is consistent with our physical understanding of the phenomenon, where a sufficiently large energy should correspond to us having gone far beyond the energy interval of the Fano resonance.

Now, what we have here is going to unfortunately be incomplete when considering the case for argon [7]. This is because here we assume that we have *one* continuum channel (as well as *one* set of bound states). However, when we do experiments with Argon we must take into account that we have *two* continuum channels for the Fano resonance we want to study. So we get one extra term that is added to the above expression for the cross-section.

$$\sigma(E) = \sigma_{bg}(E)\frac{(\epsilon + q_{\tilde{a}g})^2}{\epsilon^2 + 1} + \sigma_b, \tag{33}$$

where σ_b is this extra term. What this contribution actually is, more mathematically, will be discussed in-depth a bit later in this thesis.

3.1.2 One bound state and two continua

Now, we look at the case where we have one bound state and two continua. The reason for considering this case is due to the fact that it is relevant for the case of argon, just like how the previous discussion is of relevance to the case of helium.

The total electronic state, in this case, then becomes

$$|\Psi_{hE}\rangle = a\,|\varphi\rangle + \int \mathrm{d}\varepsilon\,[b_\varepsilon\,|\psi_\varepsilon\rangle + c_\varepsilon\,|\chi_\varepsilon\rangle] \tag{34}$$

where we now have two sets of continuum states $|\psi_\varepsilon\rangle$ and $|\chi_\varepsilon\rangle$, and the bound state is represented by $|\varphi\rangle$ once again. The index h refers to any other parameter required to characterize the final state $|\Psi_\varepsilon\rangle$ since we have a degeneracy in E now that we have two continua. Similarly to before, we consider the time-independent Schrödinger equation and the matrix elements that emerge when we project on the relevant states from the left.

$$\langle\varphi|\,H\,|\varphi\rangle = E_\varphi, \tag{35}$$

$$\langle\psi_\varepsilon|\,H\,|\varphi\rangle = V_\varepsilon, \tag{36}$$

$$\langle\chi_\varepsilon|\,H\,|\varphi\rangle = W_\varepsilon, \tag{37}$$

$$\langle\psi_{\varepsilon'}|\,H\,|\psi_\varepsilon\rangle = \langle\chi_{\varepsilon'}|\,H\,|\chi_\varepsilon\rangle = \varepsilon\delta(\varepsilon' - \varepsilon), \tag{38}$$

$$\langle\psi_{\varepsilon'}|\,H\,|\chi_\varepsilon\rangle = 0. \tag{39}$$

Treating the Schrödinger equation as before, we end up with a system of three equations:

$$E_\varphi a + \int \mathrm{d}\varepsilon\,[V_\varepsilon^* b_\varepsilon + W_\varepsilon^* c_\varepsilon] = Ea, \tag{40}$$

$$V_\varepsilon a + \varepsilon b_\varepsilon = Eb_\varepsilon, \tag{41}$$

$$W_\varepsilon a + \varepsilon c_\varepsilon = Ec_\varepsilon. \tag{42}$$

We can construct two equations by considering 41 and 42, respectively. Using that $V_\varepsilon a + \varepsilon b_\varepsilon - Eb_\varepsilon = W_\varepsilon a + \varepsilon c_\varepsilon - Ec_\varepsilon = 0$, we have:

$$V_\varepsilon^*(V_\varepsilon a + \varepsilon b_\varepsilon - Eb_\varepsilon) + W_\varepsilon^*(W_\varepsilon a + \varepsilon c_\varepsilon - Ec_\varepsilon) = 0, \tag{43}$$

which can be rewritten as

$$(\ |V_\varepsilon|^2 + |W_\varepsilon|^2)a + \varepsilon(\ V_\varepsilon^* b_\varepsilon + W_\varepsilon^* c_\varepsilon) = E(\ V_\varepsilon^* b_\varepsilon + W_\varepsilon^* c_\varepsilon). \tag{44}$$

Taking a similar linear combination, but instead with coefficients W_ε and $-V_\varepsilon$, one arrives at

$$W_\varepsilon(V_\varepsilon a + \varepsilon b_\varepsilon - E b_\varepsilon) - V_\varepsilon(W_\varepsilon a + \varepsilon c_\varepsilon - E c_\varepsilon) = 0, \tag{45}$$

which can be rewritten as

$$\varepsilon(W_\varepsilon b_\varepsilon - V_\varepsilon c_\varepsilon) = E(W_\varepsilon b_\varepsilon - V_\varepsilon c_\varepsilon). \tag{46}$$

What we do now is consider equation 40 and 44. These two together form an analogue to equations 10 and 11. Employing the same method that was used to solve for a and b_ε for the two latter equations, we solve for a and $V_\varepsilon^* b_\varepsilon + W_\varepsilon^* c_\varepsilon$ in the two new equations.

In the new case for 40 and 44, by generalizing equations 17, 18 and 25 we have

$$\overline{\Delta} = -\arctan\frac{\pi(|V_E|^2 + |W_E|^2)}{E - E_\varphi - G(E)}, \tag{47}$$

for which

$$G(E) = P\int \mathrm{d}\varepsilon \frac{|V_\varepsilon|^2 + |W_\varepsilon|^2}{E - \varepsilon}. \tag{48}$$

The coefficients then become, in analogy with equations 23 - 25,

$$a_1 = \frac{\sin\overline{\Delta}}{\sqrt{\pi(|V_E|^2 + |W_E|^2)}}, \tag{49}$$

$$b_{1\varepsilon} = \frac{V_\varepsilon}{\sqrt{|V_E|^2 + |W_E|^2}}\left[\frac{1}{\pi}\frac{\sin\overline{\Delta}}{E - \varepsilon} - \cos\overline{\Delta}\delta(E - \varepsilon)\right], \tag{50}$$

$$c_{1\varepsilon} = \frac{W_\varepsilon}{\sqrt{|V_E|^2 + |W_E|^2}}\left[\frac{1}{\pi}\frac{\sin\overline{\Delta}}{E - \varepsilon} - \cos\overline{\Delta}\delta(E - \varepsilon)\right] = \frac{W_\varepsilon}{V_\varepsilon} b_{1\varepsilon} \tag{51}$$

Once again, note how these coefficients are completely analogous to the case of one continuum. Also note the indexing for $b_{1\varepsilon}$ and $c_{1\varepsilon}$. There is another set of coefficients to be found by considering equations 40 and 46:

$$a_2 = 0, \tag{52}$$

$$b_{2\varepsilon} = \frac{W_E^*}{\sqrt{|V_E|^2 + |W_E|^2}}\delta(E - \varepsilon), \tag{53}$$

$$c_{2\varepsilon} = -\frac{V_E^*}{\sqrt{|V_E|^2 + |W_E|^2}}\delta(E - \varepsilon). \tag{54}$$

Note that $a_2 = 0$ comes from the fact that equation 46 does not couple to a.

Now, if we want to consider how dipole transitions behave, we simply get the following:

$$|\langle\Psi_E|\mathcal{O}|i\rangle|^2 = |\langle\Psi_{1E}|\mathcal{O}|i\rangle|^2 + |\langle\Psi_{2E}|\mathcal{O}|i\rangle|^2 + ... \tag{55}$$

In equation 55 above, only the first term on the right-hand side ($|\langle\Psi_{1E}|\mathcal{O}|i\rangle|^2$) actually has the Fano profile. The remaining terms simply form a constant background. This is consistent with what was said regarding equation 33, and we can identity these constant terms as contributing to the σ_b term.

3.2 Fano profile

In order to understand how the Fano resonances actually affect the transitions at hand, consider the fact that we have dipole transitions. This is because we have an electric field inducing a transition from lower to higher energy levels, and we model this with dipole transitions of the form $\langle f|\mathcal{O}|i\rangle$ where $|i\rangle$ is an arbitrary (bound) initial state and $|f\rangle$ is an arbitrary (continuum) final state. The transition amplitude, which corresponds to the probability of transition, is then $|\langle f|\mathcal{O}|i\rangle|^2$. Now, the way that Fano resonances, i.e. the presence of the bound state, affects this amplitude is simply through the multiplication of the factor $(q+\epsilon)^2/(1+\epsilon)^2$. This factor plotted against the variable ϵ can be seen, for different q parameters, in figure 7:

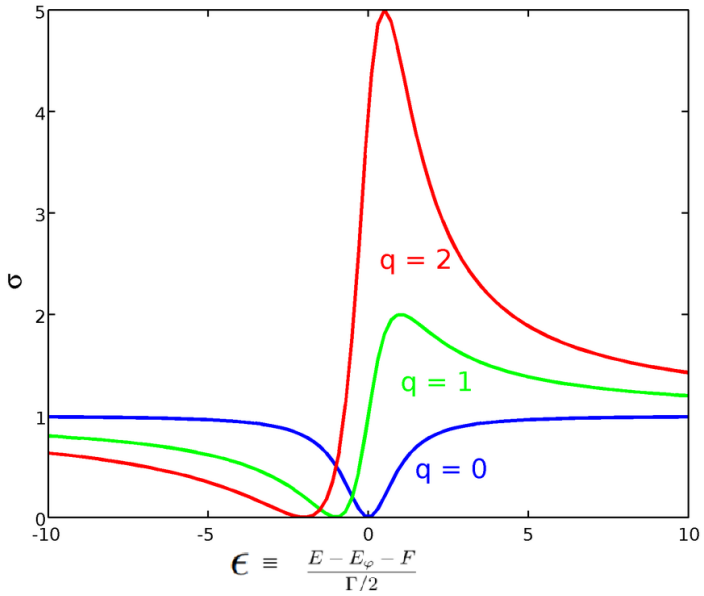

Figure 7: The absorption plotted as a function of the reduced energy, with three different plots for different values of q. The blue, symmetric, graph corresponds to $q = 0$, the green graph corresponds to $q = 1$, and the red graph corresponds to $q = 2$. Figure from [11].

In the case of argon, the q parameter is very nearly 0, which means that we approximately have the blue graph in our case (a so-called window resonance). The most important thing to consider here is the zero that the graph has. As will be seen shortly, this is what gives the desired *structure* to the EWP.

4 Spin-orbit interactions and entanglement

Next, there needs to be an explanation of how the case of argon introduces *entanglement* that justifies the use of QST. In order to undersand this, first consider the energy level diagram of the argon transitions in question, as seen in figure 8.

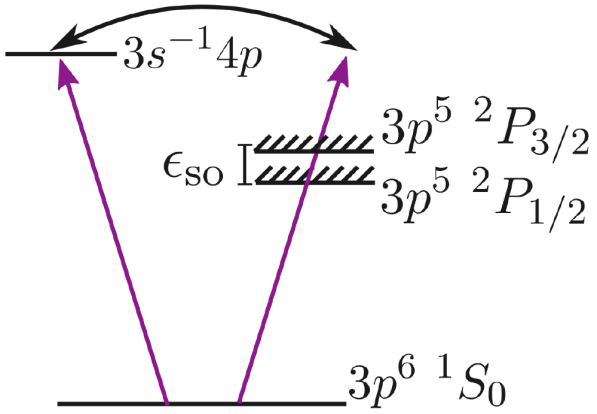

Figure 8: Energy level diagram describing the relevant transitions in the argon case study. Figure taken from [2].

The two sets of continuum energy states are separated by the spin-orbit splitting, by the energy ϵ_{so}. Spin-orbit splitting like this occur due to the electron experiencing a magnetic field due to its movement relative to the charged and stationary atomic nucleus (in this sense it is a relativistic effect). This magnetic field induces an interaction between the electron's spin (i.e. its intrinsic angular momentum) and the orbital angular momentum. In this case, the energy level of interest is split into the two levels corresponding to quantum numbers $j = 1/2$ and $j = 3/2$, respectively.

Consider the quantum state which describes both the photoelectronic state and the ionic state, namely:

$$|\Psi_{\mathrm{atom}}\rangle = c_{1/2}\,|\,j = 1/2\rangle \otimes \left|\psi_{1/2}\right\rangle + c_{3/2}\,|\,j = 3/2\rangle \otimes \left|\psi_{3/2}\right\rangle \tag{56}$$

Here the $|j = 1/2, 3/2\rangle$ states are the ionic states and the $\left|\psi_{1/2,3/2}\right\rangle$ states are the photoelectron states. When we perform measurements we only measure the photoelectron. As such, we do not interrogate ionic degrees of freedom, and this is where mixing comes in.

Mixed states can occur due to several causes. Some examples include decoherences (for example, in the light pulse used for ionization) or incomplete measurements of entangled particles [2]. In this case, we assume that the latter is the only reason for the mixing. In other words, the light pulse is assumed to be completely coherent (i.e. a pure state) and interactions with the environment are neglected. The latter of these points is motivated by the fact that we are observing processes at the attosecond time scale. For physics that fast, environmental interactions will not affect measurement results of the processes at hand.

Consider what it means to interrogate only the electronic states of $|\Psi_{\mathrm{atom}}\rangle$. The following then holds:

$$\rho_{\text{electron}} = \text{Tr}_{\text{I}}(\rho_{\text{atom}}) = \sum_j \langle j| \rho_{\text{atom}} |i\rangle \,, \; j = \frac{1}{2}, \frac{3}{2} \tag{57}$$

where

$$\rho_{\text{atom}} = |\Psi_{\text{atom}}\rangle \langle \Psi_{\text{atom}}| \tag{58}$$

and $\text{Tr}_{\text{I}}(\rho_{\text{atom}})$ denotes the trace over the *ionic degrees of freedom*. Using equation 56 and 58, and inserting them in the trace seen in equation 57, we get:

$$\rho_{\text{electron}} = |c_{1/2}|^2 \left|\psi_{1/2}\right\rangle \left\langle\psi_{1/2}\right| + |c_{3/2}|^2 \left|\psi_{3/2}\right\rangle \left\langle\psi_{3/2}\right| , \tag{59}$$

which is just a weighted sum of two density matrices, for the two respective photoelectrons. Denote these by $\rho_{1/2} = \left|\psi_{1/2}\right\rangle \left\langle\psi_{1/2}\right|$ and $\rho_{3/2} = \left|\psi_{3/2}\right\rangle \left\langle\psi_{3/2}\right|$. Both of these density matrices are identical, but shifted in energy by the spin-orbit splitting such that $\rho_{1/2}(\epsilon_1, \epsilon_2) = \rho_{3/2}(\epsilon_1 - \epsilon_{\text{so}}, \epsilon_2 - \epsilon_{\text{so}})$. Writing the sum with the correct coefficients [9], one ends up with:

$$\rho_{\text{electron}} = \frac{1}{3}\rho_{1/2} + \frac{2}{3}\rho_{3/2} \tag{60}$$

When we speak of mixing in this case, what we are interested in is whether or not these two components are spectrally resolvable. If they can both be fully resolved, there is entanglement, since a measurement on the photoelectron will tell us something about the ionic state. However, when they are not spectrally resolvable, measuring the electron does not tell us anything about the ion and we have no entanglement.

Whether or not the components are spectrally resolvable depends on the XUV bandwidth $\delta\Omega$. When we have $\delta\Omega < \epsilon_{\text{so}}$ we have fully resolvable components, which can be understood intuitively as the XUV bandwidth not "covering" both continua such that we cannot resolve the two. In the limit $\delta\Omega >> \epsilon_{\text{so}}$ however, we lose entanglement and get a pure state.

In short, the mixing is due to the incomplete measurement of only the electron degree of freedom but not the ionic degree of freedom. The entanglement is due to the spin-orbit interaction.

5 Density matrix of photoelectron wave packet

In section 3 and 4, the structure and entanglement of the EWP was discussed (Fano resonances and spin-orbit splitting, respectively). Now, it is instructive to present the actual density matrix of said EWP (for the argon transition as discussed). It is shown in figure 9 below:

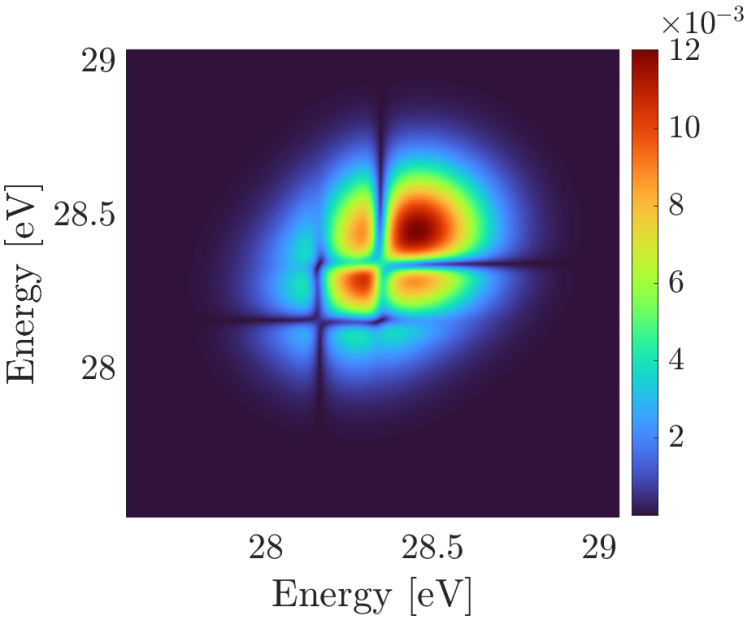

Figure 9: Amplitude of the density matrix of the argon EWP.

Note the "crosses" of zeros that can be see in the density matrix. This is the result of the Fano resonances, and gives the structure we were referring to before. Consider once again figure 7, and the zero of the curve. For each energy axis, there is going to be some energy for which the dipole transition becomes zero. This holds for every other energy on the other axis, hence the zeroes forming right angles in the density matrix.

The second thing of note is th elliptic shape of the density matrix, which is due to the entanglement. For a pure state, the density matrix would have been disk shaped, but since there is entanglement the matrix becomes elliptical. In other words, there will be less coherence between larger energy differences.

Another way of conceptualizing the elliptical appearance of the matrix is through equation 60.

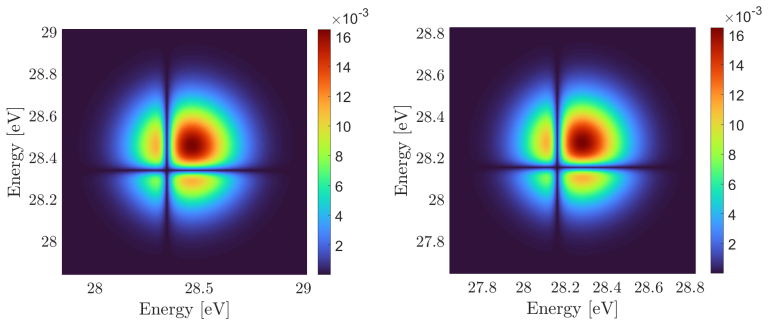

(a) $\rho_{1/2}$

(b) $\rho_{3/2}$

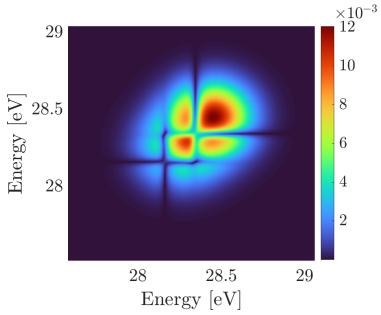

(c) ρ_{electron}

Figure 10: The argon EWP density matrix amplitude (bottom figure) as a sum of two contributions (two upper figures) due to spin-orbit splitting.

As can be seen above, the figures show the two respective spin-orbit components $\rho_{1/2}$ and $\rho_{3/2}$, which are shifted in energy relative to each other and added through a weighted sum to give the final result ρ_{electron}. If one views the final result as two discs being added together, but shifted relative to each other, it becomes intuitive that the end result would be elliptic.

6 Implementation of KRAKEN

Now, our task is to write an expression for the transition amplitude. Since we have two-photon interactions in the KRAKEN protocol, we want to begin by deriving a general expression for the transition amplitude of a two-photon transition. We use a perturbative approach. Doing this, we encounter a matrix element which requires special attention. We will finish this section by using our treatment of the two-photon matrix element to derive the two expressions for the transition amplitudes used in the simulations. These simulation results will then be presented and discussed.

What we have in this case can be seen by considering the following figure:

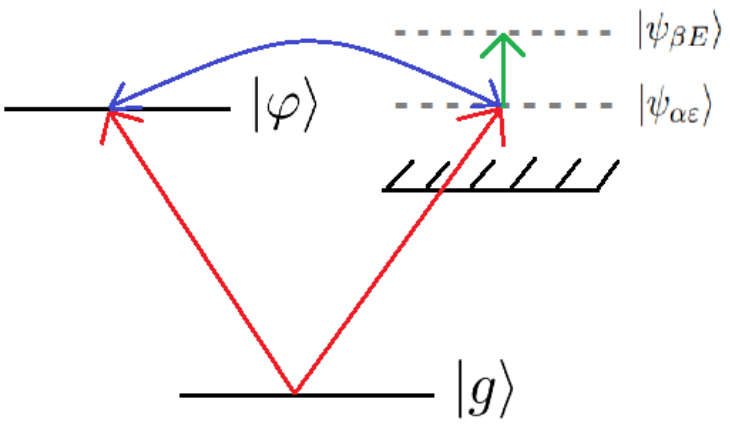

Figure 11: Energy diagram over the transitions considered in this section of the thesis. The red and green arrows correspond to the two photons in the process. The blue arrow denotes the Fano resonance between the intermediate continuum state and the bound state.

In figure 11 the physical case considered here can be seen. Note that what we are doing now is observing exclusively the two-photon transition to the continuum, i.e. the right side of the figure with the red and green arrow. The goal is to write an expression for the transition amplitude of this two-photon transition, when the intermediate state $|\psi_{\alpha\varepsilon}\rangle$ is resonant. Note the subtle difference in notation between $|\psi_{\alpha\varepsilon}\rangle$ and $|\psi_{\beta E}\rangle$. The indices α and β correspond to the two different channels. ε is the same energy variable seen before, corresponding to the continuum of energies. Meanwhile, E simply represents an energy reached by two-photon absorption. It is thus not to be confused by the energy eigenvalue E discussed in the Fano formalism.

6.1 Transition amplitude

Since KRAKEN employs a two-photon interaction with an XUV and IR photon, respectively, we need to consider the physics of two-photon transitions in order to derive expressions for the transition amplitudes.

We will approach this by considering an appropriate perturbative expression for a two-photon transition amplitude with finite pulses. And we will especially derive the expression for both time and frequency representation.

Using a dipole approximation, one can consider the standard quantum mechanical case of a target atom (or molecule) interacting with a dipole field. The

Hamiltonian will be a sum of the field-free Hamiltonian of the target as well as an interaction term, as follows [6]:

$$H(t) = H_0 + F(t)\mathcal{O},$$
$$\mathcal{O} = \hat{\epsilon} \cdot \vec{O}$$

where $H(t)$ is the total Hamiltonian of the system as a function of time t, H_0 is the field-free time-independent component and $F(t)$ is a function that essentially describes the temporal profile of the light pulse (could be a Gaussian pulse, for example). The light field is described by $\vec{F}(t) = F(t)\hat{\epsilon}$, where $\hat{\epsilon}$ is a unit vector denoting the polarization direction of the light. $\vec{O}$ is a dipole operator corresponding to the light pulse.

Assuming the system outlined above is initially in a ground state $|g\rangle$, such that $H_0 |g\rangle = \omega_g |g\rangle$. The wave function $|\psi(t)\rangle$ is then given, using the *interaction picture*, as

$$|\psi(t)\rangle = |g\rangle - i \int_{-\infty}^{t} \mathrm{d}t' F(t') \mathcal{O}_I(t') |\psi(t')\rangle \tag{61}$$

where

$$\mathcal{O}_I(t) = e^{iH(t)} \mathcal{O} e^{-iH(t)}. \tag{62}$$

Note that we will use atomic units throughout this derivation. Perturbative expansion to abritrary order then gives us:

$$|\psi(t)\rangle = \sum_{n=0}^{\infty} \left|\psi^{(n)}(t)\right\rangle, \tag{63}$$

$$\left|\psi^{(0)}(t)\right\rangle = |g\rangle, \tag{64}$$

$$\left|\psi^{(n+1)}(t)\right\rangle = -i \int_{-\infty}^{t} \mathrm{d}t' F(t') \mathcal{O}_I(t') \left|\psi^{(n)}(t')\right\rangle. \tag{65}$$

We take a close look at equations 64 and 65 and consider n=1 and n=2. For n=1 we have

$$\left|\psi^{(1)}(t)\right\rangle = -i \int_{-\infty}^{t} \mathrm{d}t' F(t') \mathcal{O}_I(t') |g\rangle. \tag{66}$$

Moving on to n=2 we get, by substituting the above expression, the following:

$$\left|\psi^{(2)}(t_2)\right\rangle = -i \int_{-\infty}^{t_2} \mathrm{d}t_2' \; F(t_2') \mathcal{O}_I(t_2') \left|\psi^{(1)}(t_2')\right\rangle \tag{67}$$

$$= -\int_{-\infty}^{t_2} \mathrm{d}t_2' \; F(t_2') \mathcal{O}_I(t_2') \int_{-\infty}^{t_2'} \mathrm{d}t_1' \; F(t_1') \mathcal{O}_I(t_1') |g\rangle \tag{68}$$

What we note here, is that for n=2, we get contribution from two pulses, i.e. pulses F centered around different times t_2 and t_1. What we can state, then, is that the lowest order for which we can describe a two-photon state using the interaction picture in a perturbative expansion is $n = 2$. Now, we consider how to mathematically write the transition amplitude. This is done by:

$$\mathcal{A}_{fg}^{(n)} = \left\langle f \middle| \psi^{(n)}(\infty) \right\rangle. \tag{69}$$

Here we have a transition to a final state $|f\rangle$, such that $H_0|f\rangle = E_f|f\rangle$. Using equation 62 we get the following:

$$\langle f|e^{iH(t_2)} = e^{i\omega_f t_2}\langle f| \tag{70}$$

$$e^{-iH(t_1)}|g\rangle = e^{-i\omega_g t_2}|g\rangle \tag{71}$$

Here, ω_f and ω_g are equivalent to the energies of the final and ground electronic states, respectively. This is because we use atomic units, and as such angular frequency and energy are equal up to $\hbar$ which is set to unity. Inserting equations 70 and 71 into equation 68, we end up with

$$\begin{aligned}
&-\int_{-\infty}^{\infty}\int_{-\infty}^{t_2} \mathrm{d}t_2'\mathrm{d}t_1'\ F(t_2')F(t_1')\langle f|\mathcal{O}_I(t_2')\mathcal{O}_I(t_1')|g\rangle \\
&= -\int_{-\infty}^{\infty}\int_{-\infty}^{t_2} \mathrm{d}t_2'\mathrm{d}t_1'\ F(t_2')F(t_1')\langle f|e^{iH(t_2')}\mathcal{O}e^{-iH(t_2')}e^{iH(t_1')}\mathcal{O}e^{-iH(t_1')}|g\rangle \\
&= -\int_{-\infty}^{\infty}\int_{-\infty}^{t_2} \mathrm{d}t_2'\mathrm{d}t_1'\ F(t_2')F(t_1')e^{i\omega_f t_2'}e^{-i\omega_g t_1'}\langle f|\mathcal{O}e^{-iH(t_2'-t_1')}\mathcal{O}|g\rangle\,.
\end{aligned}$$

In order to treat the above, we pay some special attention to $e^{-iH(t_2-t_1)}$, which can be rewritten by considering the following *Green function*:

$$G^+(t_2-t_1) = -i\theta(t_2-t_1)e^{-iH(t_2-t_1)}, \tag{72}$$

where θ is the Heaviside step function. This allows us to include the time-ordering in the integrand. Inserting this expression for the Green function into the transition amplitude, we then end up with:

$$\mathcal{A}_{fg}^{(2)} = -i\int_{-\infty}^{\infty}\int_{-\infty}^{t_2} \mathrm{d}t_2'\mathrm{d}t_1' e^{i\omega_f t_2'}e^{-i\omega_g t_1'}F(t_2')F(t_1')\langle f|\mathcal{O}G^+(t_2'-t_1')\mathcal{O}|g\rangle \tag{73}$$

Note that since we have atomic units, we can write out photon energies as being the same as their corresponding angular frequencies.

Now, we want to look at equation 73 and write its frequency representation. This will be the central mathematical expression in this section of the thesis:

$$\mathcal{A}_{fg}^{(2)} = -i\int_{-\infty}^{\infty}\mathrm{d}\omega\tilde{F}(\omega_{fg}-\omega)\tilde{F}(\omega)\mathcal{M}_{fg}(\omega) \tag{74}$$

where $\tilde{F}$ is the Fourier transform of the electric field, $\omega_{fg} = \omega_f - \omega_g$ is the energy difference in atomic units between the final and ground state, and $\mathcal{M}_{fg}$ is a two-photon transition matrix element which we can write as:

$$\mathcal{M}_{fg} = \langle f|\mathcal{O}G^+(\omega_g+\omega)\mathcal{O}|g\rangle \tag{75}$$

Here the so-called retarded resolvent $G^+(\omega)$ is the Fourier transform of G^+ and can be written as:

$$G^+(\omega) = (\omega - H + i0^+)^{-1} \tag{76}$$

In order to reach the final expression, we consider how to treat a pump-probe scheme. During a pump-probe process, the total external field is the sum of the

pump and the probe. This is written by considering the pump as $F_1(t)$ and the probe as $F_2(t;\tau) = F_2(t-\tau)$. That is, the probe field has a certain *delay* τ from the probe. What we end up with is a physical situation where the total field can be written as the following [6]:

$$F(t) = F_1(t) + F_2(t-\tau), \tag{77}$$

with the frequency representation of the above being simply given by

$$\tilde{F}(\omega) = \tilde{F}_1(\omega) + \tilde{F}_2(\omega)e^{i\omega\tau} \tag{78}$$

Using this, the following follows directly from equation 74 that one can write:

$$\mathcal{A}_{fg} = -i\int_{-\infty}^{\infty} \mathrm{d}\omega \tilde{F}_1(\omega_{fg}-\omega;\tau)\tilde{F}_2(\omega;\tau)\mathcal{M}_{fg}(\omega) \tag{79}$$

We reiterate again that the above describes a pump-probe scheme, and it is only the probe that is of interest to us in practice. After all, it is only the probe excited electron that the KRAKEN protocol aims to study. In short, the pump is the XUV pulse which is sent into the atomic gas in question. The pump excites electrons such that photoelectrons are ejected. The IR fields then probe the system in question, according to the above scheme. Keep in mind, however, that the above only takes one probe into account. Whereas for the previously described KRAKEN protocol there are two probe fields.

6.2 Two-photon transition matrix element $\mathcal{M}$

What we want to do now is examine how we can write the expression in equation 75. Here we consider the case of a Fano resonance.

6.2.1 Some general properties

Before moving on, we will examine some general properties of the matrix element $\mathcal{M}$. Indeed, this matrix element will require the lengthiest mathematical treatment in this thesis, and as such we will start with an overview. What we want to do is make an expansion in terms of the eigenstates $|\psi_{\alpha\epsilon}\rangle$, by using the completeness relation on $\mathcal{M}_{fg}$ [6]. Using the fact that α corresponds to a discrete set of states and ε is our continuous energy variable,

$$\int \mathrm{d}\varepsilon \, |\psi_{\alpha\varepsilon}\rangle \langle\psi_{\alpha\varepsilon}| = 1. \tag{80}$$

Note that we here only consider one channel α, as opposed to summing over many different such channels. We also do not consider any additional bound states below the continuum, in which case using the symbol $\not\int$ would be more appropriate than the integral sign. These approximations will be discussed shortly. Inserting the completeness relation in equation 80 into the expression

for $\mathcal{M}$ seen in equation 75, we get

$$\begin{aligned}\mathcal{M}_{fg} &= \int \mathrm{d}\varepsilon \langle f|\mathcal{O}|\psi_{\alpha\varepsilon}\rangle \langle\psi_{\alpha\varepsilon}|G^{+}(\omega_g+\omega)\mathcal{O}|g\rangle \\ &= \int \mathrm{d}\varepsilon \langle f|\mathcal{O}|\psi_{\alpha\varepsilon}\rangle \langle\psi_{\alpha\varepsilon}|\frac{1}{\omega+\omega_g-H+i0^{+}}\mathcal{O}|g\rangle .\end{aligned}$$

Now, we can use the fact that $H|\psi_{\alpha\varepsilon}\rangle = \epsilon|\psi_{\alpha\varepsilon}\rangle$ as well as $\langle f|\mathcal{O}|\psi_{\alpha\varepsilon}\rangle = \mathcal{O}_{f,\alpha\varepsilon}$ and $\langle\psi_{\alpha\varepsilon}|\mathcal{O}|g\rangle = \mathcal{O}_{\alpha\varepsilon,g}$ to arrive at

$$\mathcal{M}_{fg}(\omega) = \int \mathrm{d}\varepsilon \frac{\mathcal{O}_{f,\alpha\varepsilon}\mathcal{O}_{\alpha\varepsilon,g}}{\omega_g+\omega-\varepsilon+i0^{+}}. \tag{81}$$

6.2.2 $\mathcal{M}$ for one continuum

What we want to do now is consider how the matrix element $\mathcal{M}$ behaves for our specific cases, i.e. helium and argon, respectively. We start by considering helium, in which case we only need to consider one continuum.

Writing the general expression for $\mathcal{M}$ for this case we get:

$$\mathcal{M}_{\beta E,g}(\omega) = \int \mathrm{d}\varepsilon \frac{\langle\psi_{\beta E}|\mathcal{O}|\psi_{\alpha\varepsilon}\rangle\langle\psi_{\alpha\varepsilon}|\mathcal{O}|g\rangle}{\omega_g+\omega-\varepsilon+i0^{+}} \tag{82}$$

Now, our task is to rewrite equation 82 to a more manageable form, which can be done using equation 31, since the dipole transition is subject to Fano resonances:

$$\langle\psi_{\alpha\varepsilon}|\mathcal{O}|g\rangle = \frac{\epsilon_{\varepsilon a}+q_{\tilde{a}g}}{\epsilon_{\varepsilon a}+i}\mathcal{O}_{\alpha\varepsilon,g}, \tag{83}$$

where, just like in our original discussion of Fano resonances, we have the dipole transition matrix element to the continuum states of the α channel ($\mathcal{O}_{\alpha\epsilon,g}$) modified by the bound state. This gives the rational expression, containing the q parameter, as a factor. Substitution of this expression in equation 82 gives us

$$\mathcal{M}_{\beta E,g}(\omega) = \int \mathrm{d}\varepsilon \frac{\langle\psi_{\beta E}|\mathcal{O}|\psi_{\alpha\varepsilon}\rangle}{\omega_g+\omega-\varepsilon+i0^{+}}\frac{\epsilon_{\varepsilon a}+q_{\tilde{a}g}}{\epsilon_{\varepsilon a}-i}\mathcal{O}_{\alpha\varepsilon,g} \tag{84}$$

Now, what we need to do is consider what happens with the dipole transition $\langle\psi_{\beta E}|\mathcal{O}|\psi_{\alpha\epsilon}\rangle$. Unlike expression 31, here we have a transition from a continuum state to another continuum state. The derivation of this dipole transition matrix element is complicated, and we refer to the original paper by Jímenez-Galán for a more complete treatment [6].

What we will do here is simply state that the expression in equation 84 can be written as follows

$$\mathcal{M}_{\beta E,g}(\omega) = \frac{\epsilon_{Ea}+q_{\tilde{a}g}}{\epsilon_{Ea}+i}\frac{\overline{\mathcal{O}}_{\beta\alpha}\mathcal{O}_{\alpha,g}}{\omega_g+\omega-E+i0^{+}} \tag{85}$$

$$+\left(\beta_a-\frac{1}{\epsilon_{Ea}+i}\right)(q_{\tilde{a}g}-i)\frac{\overline{\mathcal{O}}_{\beta\alpha}\mathcal{O}_{\alpha,g}}{\omega-\omega_{\tilde{a}g}}, \tag{86}$$

where we have introduced the parameter $\beta_a = \pi \mathcal{O}_{\beta,a} V_{a\alpha} / \overline{\mathcal{O}}_{\beta\alpha}$. The above can now be inserted into the integral expression 74 which gives us our final expression for the transition amplitude. But before that, we need to look at a special function that needs to be employed here [6].

In the above expressions, we have introduced $\overline{\mathcal{O}}_{\beta\alpha}(E)$, which we define as the integral of the actual transition amplitude $\mathcal{O}_{\beta E,\alpha\varepsilon}$ over a small energy interval:

$$\overline{\mathcal{O}}_{\beta\alpha}(E) = \int_{E-\delta}^{E+\delta} \mathrm{d}\varepsilon \ \langle \psi_{\beta E} | \mathcal{O} | \psi_{\alpha\varepsilon} \rangle \tag{87}$$

For a deeper understanding of this, we once again refer to the Jímenez-Galán paper [6]. For the purposes of this thesis, the form with the overline (on the left-hand side of equation 87) is the only one that needs to be considered.

6.2.3 Faddeeva function formalism

Now that we have arrived at a useful expression for $\mathcal{M}$, we need to examine one more aspect of the transition amplitude $\mathcal{A}$ before the final expression can be presented. For the purpose of manageable numerics, special functions were employed, and the formalism will be discussed here. We begin by writing equation 74 on the following form [6]:

$$\mathcal{A}_{fg} = -i \int_{\infty}^{\infty} \mathrm{d}\omega \tilde{F}_2(\omega_{Eg} - \omega; \tau) \tilde{F}_1(\omega) \mathcal{M}_{\beta E,g}(\omega) \tag{88}$$

The physical interpretation of equation 88 above is that we have a two-photon transition from an initial state $|g\rangle$ with energy ω_g, to a final state $|\beta E\rangle$ with energy E. This process occurs through an absorption/emission of a photon (here labeled 1) which we consider as a Gaussian pulse of shape F_1, with frequency ω_1, centered around $t_1 = 0$, and a subsequent absorption/emission of a photon labeled 2, as a Gaussian pulse of shape F_2 (with frequency ω_2) centered around $t_2 = t_1 + \tau = \tau$. We proceed by considering the following treatment of the matrix element $\mathcal{M}$, as seen in the Appendix of the Jímenez-Galán paper [6]:

$$\mathcal{M}_{\beta E,g}(\omega) \sim \frac{1}{\omega - \omega_{ag}} \tag{89}$$

In order to continue, one can rewrite equation 88 in a more general form without the integral. The fields in question are assumed to be Gaussian, so one ends up with the following ($n = 1,2$):

$$\begin{aligned}
\widetilde{F}_n(\omega) &= \int F_n(t) e^{i\omega t} \, \mathrm{d}t \\
&= F_n \int e^{-\sigma_n^2 (t-t_n)^2/2} \cos\left[\omega_n (t - t_n)\right] e^{i\omega t} \, \mathrm{d}t \\
&= F_n \int e^{-\sigma_n^2 (t-t_n)^2/2} \frac{1}{2} \left[e^{i[\omega_n (t-t_n)]} + e^{-i[\omega_n (t-t_n)]} \right] e^{i\omega t} \, \mathrm{d}t,
\end{aligned}$$

where F_n is the amplitude of the field (the n:th pulse), ω_n is the central frequency, t_n is the starting time and σ is the temporal pulse width. Note especially

that the expression substituted for $F_n(t)$ is simply a standard representation of a Gaussian pulse in the time domain. The integral above splits into two terms, which correspond to absorption and emission, respectively. The exponent with the negative sign corresponds to absorption and the one with the positive sign corresponds to emission. Since we are only interested in absorption, we choose to study the negative term exclusively. Thus we only consider the following contribution:

$$\widetilde{F}_n(\omega) = \frac{F_n}{2} \int e^{-\sigma_n^2 (t-t_n)^2/2} e^{-i[\omega_n (t-t_n)]} e^{i\omega t} \, \mathrm{d}t. \tag{90}$$

We perform a variable substitution by shifting the integration variable by $+t_0$, which gives a more manageable form of the above expression. We will also perform yet another substitution. All of this is done as follows:

$$\widetilde{F}_n(\omega) = \frac{F_n}{2} e^{i\omega t_n} \int \exp\left\{-\sigma_n^2 t^2/2 - i\omega_n t - i\omega t\right\} \, \mathrm{d}t. \tag{91}$$

Using the substitution $u = \sigma_n t/\sqrt{2}$ we get

$$\widetilde{F}_n(\omega) = \frac{F_n}{2} \frac{\sqrt{2}}{\sigma_n} e^{i\omega t_n} \int \exp\left\{-\left[u^2 + i\frac{\sqrt{2}}{\sigma_n}(\omega - \omega_n)u\right]\right\} \mathrm{d}u \tag{92}$$

$$= \frac{F_n}{2} \frac{\sqrt{2}}{\sigma_n} e^{i\omega t_n} \int \exp\left\{-\left[\left(u + i\frac{1}{\sqrt{2}\sigma_n}(\omega - \omega_n)\right)^2 + \frac{1}{2\sigma_n^2}(\omega - \omega_n)^2\right]\right\} \mathrm{d}u \tag{93}$$

$$= \sqrt{\frac{\pi}{2}} \frac{F_n}{\sigma_n} e^{i\omega t_n} \exp\left\{-\frac{1}{2\sigma_n^2}(\omega - \omega_n)^2\right\} \tag{94}$$

By inserting equation 94 and 89 into 88 we arrive at one of the key expressions of this thesis:

$$\mathcal{A}_{fg} = -i \int_{-\infty}^{\infty} \mathrm{d}\omega \; \tilde{F}_2(\omega_{fg} - \omega;\; \tau) \tilde{F}_1(\omega) \frac{1}{\omega - \omega_{ag}} \tag{95}$$

$$= -\frac{i\pi}{2} \frac{F_2 F_1}{\sigma_2 \sigma_1} \int_{\infty}^{\infty} \mathrm{d}\omega \; \frac{e^{-i(\omega_{Eg} - \omega)\tau}}{\omega - \omega_{ag}} e^{-\frac{(\omega_{Eg} - \omega - \omega_2)^2}{2\sigma_2^2}} e^{-\frac{(\omega - \omega_1)^2}{2\sigma_1^2}} \tag{96}$$

What is done in the Jiménez-Galan paper, then, is rewriting equation 96 so that we can employ special functions for the purpose of easier numerical treatment. Specifically we use the *Faddeeva* function, which can be written with the following integral form [6]:

$$w(z) = \frac{i}{\pi} \int_{-\infty}^{+\infty} \mathrm{d}t \frac{e^{-t^2}}{z - t}, \; \mathrm{Im}(z) > 0 \tag{97}$$

So we want to rewrite the integral expression using 97. The following form is from the Jímenez-Galan paper [6], and will be presented here without further

explanation:

$$\mathcal{A}_{fg} = -\frac{i\pi}{2}\frac{F_2F_1}{\sigma_2\sigma_1}\exp\left(-\frac{\delta^2}{2\sigma^2}-\frac{\tau^2}{2\sigma_t^2}-i\frac{\sigma_2}{\sigma_1}\frac{\tau}{\sigma_t}\frac{\delta}{\sigma}+i\omega_2\tau\right) \times \int_{\infty}^{\infty} \mathrm{d}\omega \frac{\exp\left[-\frac{1}{2}\left(\sigma_t\omega+\frac{\sigma_1}{\sigma_2}\frac{\delta}{\sigma}+i\frac{\tau}{\sigma_t}\right)^2\right]}{\omega_1+\omega-\omega_{ag}}$$

Here we have introduced some new variables defined by $\sigma = \sqrt{\sigma_1^2+\sigma_2^2}$, $\sigma_t = \sqrt{\sigma_1^{-2}+\sigma_2^{-2}}$ and $\delta = \omega_g + \omega_1 + \omega_2$ - E. Note that E here is not the same as ω. The latter is our integration variable and the value E denotes the continuum state energy corresponding to the state $|\beta E\rangle$. This rewrite is performed in the paper by Jímenez-Galán [6], and will not be demonstrated in detail in this thesis. By comparing the above to the expression in equation 97, we find the following:

$$z_a = \frac{\sigma_t}{\sqrt{2}}\left[\omega_1 - \frac{\sigma_1^2}{\sigma}\delta - i\frac{\tau}{\sigma_t^2} - \omega_{ag}\right] \tag{98}$$

Again, we refer to the Jímenez-Galán paper for this result [6]. So we have the Faddeeva function formulation of the integral expression for the transition amplitude, and we thus finally arrive at the following:

$$\begin{aligned}\mathcal{A}_{fg} &= -\frac{\pi^2}{2}\frac{F_2F_1}{\sigma_2\sigma_1}e^{-i\omega_2\tau} \\ &\times \exp\left(-\frac{\delta^2}{2\sigma^2}-\frac{\tau^2}{2\sigma_t^2}-i\frac{\sigma_2}{\sigma_1}\frac{\tau}{\sigma_t}\frac{\delta}{\sigma}+i\omega_2\tau\right)w(z_a) \\ &= \mathcal{F}(\tau)w(z_a)\end{aligned}$$

where we in $\mathcal{F}(\tau)$ collect all of the terms in front of the Faddeeva function.

6.2.4 Final expression

We now insert equation 86 into equation 74 to arrive at the final expression of the transition amplitude:

$$\begin{aligned}\mathcal{A}_{fg} &= -i\int_{-\infty}^{\infty}\mathrm{d}\omega\tilde{F}(\omega_{fg}-\omega)\tilde{F}(\omega)\mathcal{M}_{fg}^{(2)}(\omega) \\ &= -i\int_{-\infty}^{\infty}\mathrm{d}\omega\tilde{F}(\omega_{fg}-\omega)\tilde{F}(\omega) \\ &\times \left[\frac{\epsilon_{Ea}+q_{\tilde{a}g}}{\epsilon_{Ea}+i}\frac{\overline{\mathcal{O}}_{\beta\alpha}\mathcal{O}_{\alpha,g}}{\omega_g+\omega-E+i0^+}+\left(\beta_a-\frac{1}{\epsilon_{Ea}+i}\right)(q_{\tilde{a}g}-i)\frac{\overline{\mathcal{O}}_{\beta\alpha}\mathcal{O}_{\alpha,g}}{\omega-\omega_{\tilde{a}g}}\right] \\ &= -i\frac{\epsilon_{Ea}+q_{\tilde{a}g}}{\epsilon_{Ea}+i}\overline{\mathcal{O}}_{\beta\alpha}\mathcal{O}_{\alpha,g}\int_{-\infty}^{\infty}\mathrm{d}\omega\tilde{F}(\omega_{fg}-\omega)\tilde{F}(\omega)\frac{1}{\omega_g+\omega-E+i0^+} \\ &- -i\left(\beta_a-\frac{1}{\epsilon_{Ea}+i}\right)(q_{\tilde{a}g}-i)\overline{\mathcal{O}}_{\beta\alpha}\mathcal{O}_{\alpha,g}\int_{-\infty}^{\infty}\mathrm{d}\omega\tilde{F}(\omega_{fg}-\omega)\tilde{F}(\omega)\frac{1}{\omega-\omega_{\tilde{a}g}}\end{aligned}$$

Thus one gets two terms, and each of these can be rewritten using the Faddeeva function, except with z_E being dependent on a different E for the two terms, due to the differences in their respective integrands' denominators. The final expression for the transition amplitude then becomes

$$\mathcal{A}_{\beta E,g} = \mathcal{F}(\tau)e^{i\omega_2\tau}\overline{\mathcal{O}}_{\beta\alpha}\mathcal{O}_{\alpha E,g} \times \left[\frac{\epsilon_{Ea}+q_{\tilde{a}g}}{\epsilon_{Ea}+i}w(z_E) + \left(\beta_a - \frac{1}{\epsilon_{Ea}+i}\right)(q_{\tilde{a}g}-i)w(z_{\tilde{E}_a})\right]$$

We want to employ some approximations to further simplify the above expression, which will give us the final expression we consider. The approximation we consider is simply that we have $\epsilon_{Ea} >> i$ as well as $\epsilon_{Ea} >> q_{\tilde{a}g}$. This gives us

$$\mathcal{A}_{\beta E,g} = \mathcal{F}(\tau)e^{i\omega_2\tau}\overline{\mathcal{O}}_{\beta\alpha}\mathcal{O}_{\alpha E,g}\left[w(z_E) + (\beta_e - \epsilon_{Ea}^{-1})(q_{\tilde{a}g}-i)w(z_{\tilde{E}_a})\right], \tag{99}$$

which is the final expression that will be considered for the transition amplitude, and the one to be used in the simulations.

6.3 Simulations

Here we present the result of simulations performed using equation 99. The code was written by David Busto, and the input parameters in question are chosen as follows: the resonance energy is set to 26.6 eV, the q parameter is set to -0.25, $\Gamma_{\text{res}} = 0.076$ eV, and an IR wavelength of 790 nm, as well as an IR bandwidth of 7 nm. For the XUV pulse we have a detuning of 0.05 eV and a bandwidth of 0.1 eV.

We then get:

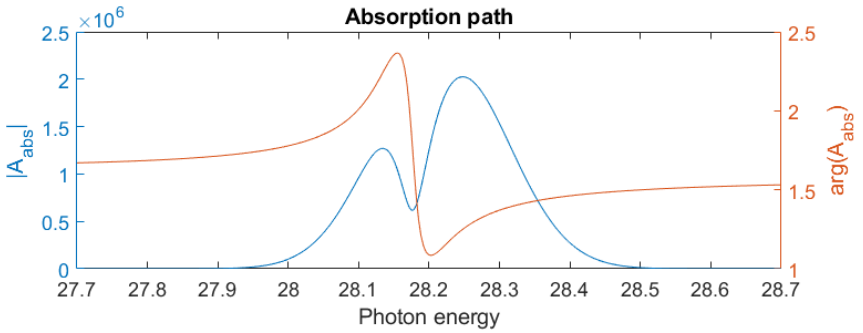

Figure 12: Simulation results for the parameters discussed above. The most interesting part here is the blue graph, which shows the modules of the amplitude. The orange graph, in contrast, shows the phase.

In figure 12 we see the amplitude modules for the absorption as blue graph, and the phase as an orange graph.

7 Simulations and limitations of KRAKEN

In this section the KRAKEN simulations will be examined in more detail, before the possible extensions of KRAKEN are discussed. At first, we will demonstrate that simulating KRAKEN actually does give the desired density matrix to a very high fidelity. After that, the limitations of KRAKEN will be discussed. In particular, the effects of the IR bandwidth on the sampling will be examined.

7.1 KRAKEN simulations

Now that the theory of two-photon transitions has been presented, and the expression for the transition amplitude derived, we are ready to see how the results of actual KRAKEN simulations.

Consider the case of Helium, where we have no entanglement due to the absence of spin-orbit splittings and as such no state mixing occurs when measuring the photoelectron state. The result is a pure state, but the principles of recovering the density matrix remains the exact same.

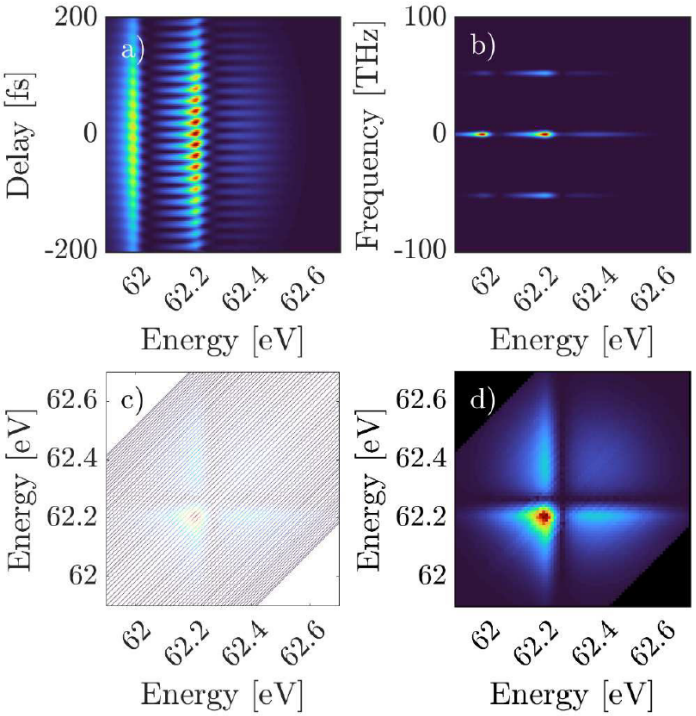

Figure 13: Constructing the density matrix from a KRAKEN simulation. Figure taken from [2].

Consider figure 13 above. In the top left, we have at first the sideband of a

scan, compare with the experimental data in figure 4 b). This data corresponds to $S(\epsilon, \tau, \delta\omega)$, and in the top right figure we can see the Fourier transformed data. From this the desired frequency component is extracted, and performing this over and over one recovers the subdiagonals seen in the bottom left of figure 13. This data is then interpolated to give a clearer picture of the density matrix, which can be seen in the bottom right.

In order to examine the fidelity of this simulation, the end result can be compared with a density matrix acquired through a direct calculation. That is, simply computing 58 directly and plotting the resulting matrix. The result of this can be seen in figure 14 below. The top figure is the one from the direct calculation and the bottom figure is from the KRAKEN simulation. As can be seen, the two are near identical which indicates that the KRAKEN simulation is indeed quite robust.

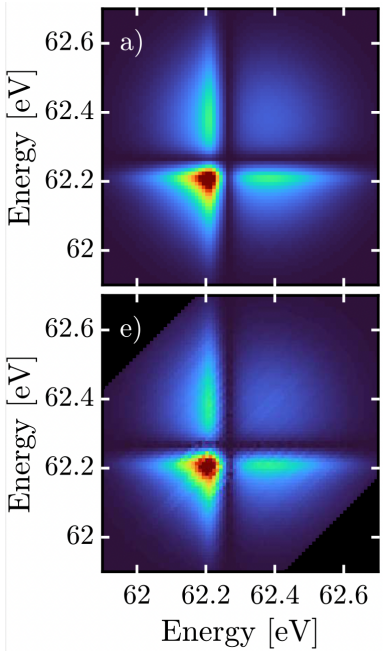

Figure 14: Comparison of KRAKEN simulation and direct calculation for the amplitude of the density matrix of a helium EWP. The upper figure is the direct calculation and bottom figure is the KRAKEN simulation. Figure taken from [2].

7.2 Limitations of KRAKEN

Now, consider the effects of IR bandwidth on the KRAKEN simulations. Again, the case of Helium is considered. Initially in the simulations, both of the IR probes have IR bandwidths of 1.5 nm, which is approximately monochromatic.

Then, one of the two IR probes is increased to 5, 10 and 20 nm, while the other is kept at 1.5 nm. The results can be seen n figure

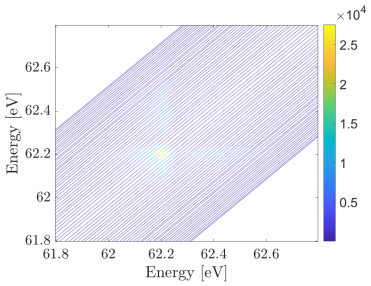

(a) Both probes with bandwidth 1.5 nm.

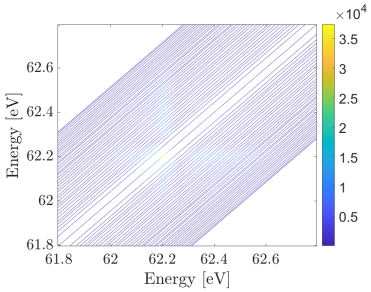

(b) One IR probe with bandwidth 1.5 nm and the other with bandwidth 5 nm.

Figure 15

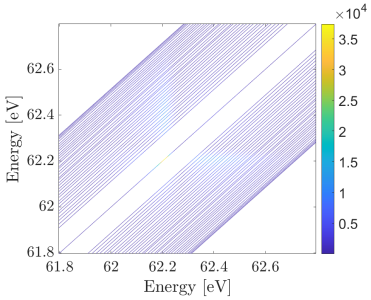

(a) One IR probe with bandwidth 1.5 nm and the other with bandwidth 10 nm.

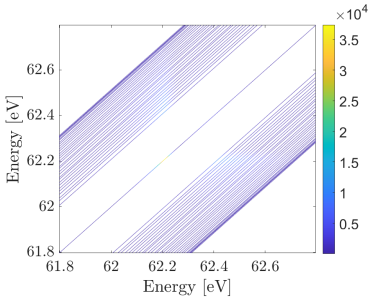

(b) One IR probe with bandwidth 1.5 nm and the other with bandwidth 20 nm.

Figure 16

As can be seen here, as the bandwidth of one of the IR probes increases, there is an increasing region of information loss around the main diagonal. In order to understand this behaviour, consider what it means for the pulses to be Fourier limited. In this case, the most important consequence of the pulses being Fourier limited is that the bandwidth is inversely proportional to the *pulse duration*. So the broader the IR pulse becomes spectrally, the shorter its temporal duration. Recall how the simulations are actually performed: in order to acquire the transition amplitude $\mathcal{A}$, a convolution between the two pulses (and also the $\mathcal{M}$ dipole transition matrix element) has to be computed. Consider the coherences around the main diagonal (which is where the information loss occured). There the energy differences considered, i.e. between ϵ_1 and ϵ_2 are small (they are

zero on the main diagonal). A small energy difference corresponds to a long time. I.e. when taking the autocorrelation there is a longer time required to actually recover the information. However, if the pulse duration is short (due to the longer IR bandwidth) there is a possibility that the pulse is too short in duration to scan over the energy difference. I.e. the pulse is too short to capture all the information needed. This leads to information loss, and as the IR pulse becomes broader the more coherences it becomes unable to recover. Hence the growing information gap.

It is also important to understand that this is not a component of the physics itself, but rather the sampling. This is lost information, which is impossible to recover due to the sampling theorem. As such, this is a fundamental limitation of the data analysis that KRAKEN requires to work.

8 Single-pulse KRAKEN

The second limitation of KRAKEN we consider is the fact that it is very experimentally demanding. What is meant by this is that KRAKEN takes a very long time to perform (the order of magnitude here is dozens of hours). This is because one scan is performed for each bichromatic IR pulse, to acquire one subdiagonal at a time. The idea here is to examine if KRAKEN could be made much quicker by employing a *single IR pulse* that could allow us to recover all subdiagonals, as opposed to each IR pulse corresponding to the acquisition of only one subdiagonal.

Two approaches to this idea were investigated. The first was to have a chirped IR pulse, and the other was to employ an IR pulse with a square spectrum. Both of these will be discussed in detail here.

8.1 Chirped pulse

The first extension of KRAKEN that we examine in this thesis is adding a chirp, i.e. a temporal variation of the frequency, to one of the IR probe fields. The main idea here is, as we outlined before, to examine whether the scan of frequencies can be replaced by the use of a chirped pulse. The mathematical treatment presented here will be analogous to sections 6.2.3 and 6.2.4. We examine how adding chirp changes the final expression for the transition amplitude that is to be employed numerically.

In figure 17 below the situation at hand can be seen, with the previous case for KRAKEN discussed in section 2 contrasted with the chirped case to be studied here.

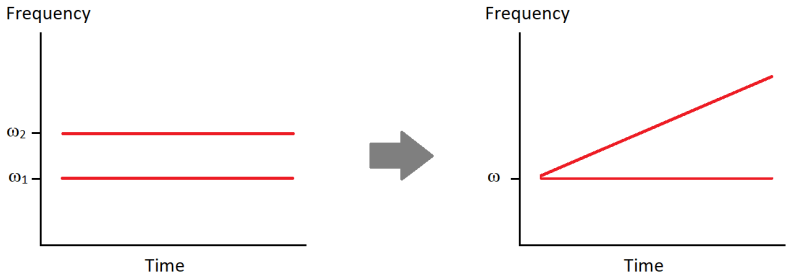

Figure 17: Time-frequency graphs describing the bichromatic IR probe field. In the left figure, we have two monochromatic pulses represented by constant frequencies in time. To the right we have added linear chirp to one of the pulses, so it becomes a straight line in the time-frequency plane. The other probe pulse remains unchirped.

So we have two IR pulses above and give one of them a chirp, i.e. the instantaneous frequency is a straight line with an incline specified by a chirp parameter.

8.1.1 Implementation of chirp

To understand the effect of adding a chirp to the pulse, the derivations and results acquired in the paper by Jímenez-Galán were studied in detail. We start by writing the chirped Gaussian in the following form [10], where we analogously to the previous discussion have the two pulses denoted by $n = 1,2$:

$$F_n(t) = F_n e^{-\sigma_n^2 (t-t_n)^2/2} \cos\left[\omega_n(t-t_n) + \beta_n(t-t_n)^2\right], \ n = 1,2. \tag{100}$$

and also

$$\beta_1 = 0, \ \beta_2 \neq 0, \tag{101}$$

since only one of the probe fields is chirped.

This is simply the expression for a Gaussian pulse profile but with a chirp added, as seen by the extra phase term $\beta_n(t-t_n)^2$. Similarly to before, F_n is the amplitude of the pulse, σ_n is the temporal width, ω_n is the central frequency of the pulse, t_n is a constant time and β_n is the so-called *chirp parameter*. This means that we get an instantaneous angular frequency given by (here $\phi_n(t)$ is the phase)

$$\frac{\mathrm{d}\phi_n}{\mathrm{d}t} = \omega_n + 2\beta_n(t-t_n),$$

such that a straight line of slope $2\beta_n$ specifies how quickly the instantaneous angular frequency changes as a function of time. In order to find the transition amplitude, we simply use this new chirped Gaussian to perform a derivation analogous to the one in section 3.

Considering only the absorption term:

$$\widetilde{F}_n(\omega) = \frac{F_n}{2}\int \exp\left\{-\sigma_n^2(t-t_n)^2/2 - i[\omega_n(t-t_n)+\beta_n(t-t_n)^2] + i\omega t\right\}\,\mathrm{d}t \tag{102}$$

We then perform substitutions of the same kind as was done to compute the integrals for the Faddeeva function. We thus end up with an expression analogous to the one we have seen before:

$$\begin{aligned}
&\frac{F_n}{2}e^{-i\omega t_n}\int \exp\left\{-\sigma_n^2 t^2/2 - i[\omega_n t+\beta_n t^2] + i\omega t\right\}\,\mathrm{d}t \\
&= \frac{F_n}{2}\frac{\sqrt{2}}{\sigma_n}e^{-i\omega t_n}\int \exp\left\{-(1+i2\beta_n/\sigma_n^2)u^2 + i\frac{\sqrt{2}}{\sigma_n}(\omega-\omega_n)u\right\}\,\mathrm{d}u \\
&= \frac{F_n}{2}\frac{\sqrt{2}}{\sigma_n}e^{-i\omega t_n}\int \exp\left\{-(1+i2\beta_n/\sigma_n^2)\left[u^2 - \frac{i\frac{\sqrt{2}}{\sigma_n}(\omega-\omega_n)}{1+i2\beta_n/\sigma_n^2}u\right]\right\}\,\mathrm{d}u
\end{aligned}$$

We treat the above by performing completion of the square for the expression inside the exponential. Doing this we get

$$\begin{aligned}
&\frac{F_n}{2}\frac{\sqrt{2}}{\sigma_n}e^{i\omega t_n}\int \exp\left\{-(1+i2\beta_n/\sigma_n^2)\left[\left(u - \frac{i(\omega-\omega_0)}{\sqrt{2}\sigma_n(1+i2\beta_n/\sigma_n^2)}\right)^2 + \frac{(\omega-\omega_n)^2}{2\sigma_n^2(1+i2\beta_n/\sigma_n^2)^2}\right]\right\}\,\mathrm{d}u \\
&= \frac{F_n}{\sqrt{2}\sigma_n}e^{i\omega t_n}\exp\left\{\frac{-(\omega-\omega_n)^2}{2\sigma_n^2(1+i2\beta_n/\sigma_n^2)}\right\}\frac{\sqrt{\pi}}{\sqrt{1+i2\beta_n/\sigma_n^2}}.
\end{aligned}$$

We introduce $g_n = \sigma_n^2(1+i2\beta_n/\sigma_n^2)$ so that we can rewrite the above as follows:

$$\frac{F_n}{\sqrt{2}}e^{i\omega t_n}\exp\left\{\frac{-(\omega-\omega_n)^2}{2g_n}\right\}\sqrt{\frac{\pi}{g_n}} \tag{103}$$

Now, we can finally consider equation 79 since we have arrived at an expression for the integrand. We get the following:

$$\mathcal{A}_{\beta E,g} = \frac{\pi F_2 F_1}{4\sqrt{g_1 g_2}}\int \frac{1}{\omega-\omega_{ag}}e^{i(\omega_{Eg}-\omega)\tau}e^{-(\omega_{Eg}-\omega+\omega_2)^2/2g_2}e^{-(\omega+\omega_1)^2/2g_1}\mathrm{d}\omega \tag{104}$$

Note that equation 104 is on the same form as equation 96, except σ_n has been substituted with $\sqrt{g_n}$. This allows us to immediately consider the Faddeeva function formalism, as long as the substitution of σ_n is made. Doing this we arrive at the following:

$$\mathcal{A}_{\beta E,g} = -\frac{i\pi}{2}\frac{F_2F_1}{4\sqrt{g_2g_1}}\exp\left(-\frac{\delta^2}{2\sigma^2} - \frac{\tau^2}{2\sigma_t^2} - i\sqrt{\frac{g_2}{g_1}}\frac{\tau}{\sigma_t}\frac{\delta}{\sigma} + i\omega_2\tau\right) \tag{105}$$

$$\times\int_\infty^\infty \mathrm{d}\omega\frac{\exp\left[-\frac{1}{2}\left(\sigma_t\omega + \sqrt{\frac{g_1}{g_2}}\frac{\delta}{\sigma} + i\frac{\tau}{\sigma_t}\right)^2\right]}{\omega_1+\omega-\omega_{ag}} \tag{106}$$

$$= \frac{\pi^2}{2}\frac{F_2F_1}{4\sqrt{g_2g_1}}\exp\left(-\frac{\delta^2}{2\sigma^2} - \frac{\tau^2}{2\sigma_t^2} - i\sqrt{\frac{g_2}{g_1}}\frac{\tau}{\sigma_t}\frac{\delta}{\sigma} + i\omega_2\tau\right)w(z_a) \tag{107}$$

$$= \mathcal{F}(\tau)w(z_a) \tag{108}$$

where we have that

$$z_a = \frac{\sigma_t}{\sqrt{2}}\left[\omega_1 - \frac{g_1}{\sigma^2}\delta - i\frac{\tau}{\sigma_t^2} - \omega_{ag}\right],\ \mathrm{Im}(z_a) > 0$$

as well as $\sigma = \sqrt{g_1 + g_2}$ and $\sigma_t = \sqrt{g_1^{-1} + g_2^{-1}}$. Now we can simply follow the same steps as demonstrated in section 4, since the matrix element $\mathcal{M}$ is not affected by the pulse shape $F_n(t)$. And it is the pulse shape that is actually affected by the chirp.

So we simply end up with

$$\mathcal{A}_{\beta E,g} = \mathcal{F}(\tau)\left(w(z_a) + (\beta_e - \varepsilon_{Ea}^{-1})(q_{\tilde{a}g} - i)w(z_{\tilde{E}_a})\right),$$

8.1.2 Outlook on the chirp method

While the above mathematics are deemed to be robust, there still has not been enough work done on simulations for any results to be presented on the matter. More work thus needs to be done.

8.2 Square spectrum

Now the effects of bandwidth, and how to treat the data given these effects, are to be examined. To start, consider what happens to the interaction Hamiltonian when we take into account that we do not have monochromatic light, but rather broadband radiation centered around our frequency of interest.

Consider the previously shown derivation of the KRAKEN protocol. If one observes just one of the two probe fields, the interaction Hamiltonian due to the IR field can be written as

$$\mathcal{H}_{ir}(t) = \frac{\hbar}{\sqrt{2\pi\sigma^2}} f(t) e^{i\omega(t+\tau)} \Pi_\omega. \tag{109}$$

where the Gaussian pulse shape has been replaced with a more general $f(t)$. Moving forward, $f(t)$ will be chosen so that we have a *rectangular pulse* in the frequency domain, which would imply a sinc function in temporal representation, though the specifics of the temporal shape are not of interest here. The reason for this choice of pulse shape will become clear in the following derivations. It should also be noted that rectangular pulse shapes are a decent approximation of the kind of pulses employed, perhaps even more so than the Gaussian shape.

The pulse shape in frequency representation is

$$f(\omega) = \theta(\omega - \omega_0 + \sigma_\omega/2) - \theta(\omega - \omega_0 - \sigma_\omega/2),$$

where ω_0 is the central frequency and σ_ω denotes the spectral width.

Considering an analogue to the derivation of the KRAKEN protocol, we have the following:

$$\langle\varepsilon|\,\rho_{\text{xuv+ir}}\,|\varepsilon\rangle = \langle\varepsilon|\,\rho_{\text{xuv}}\,|\varepsilon\rangle + \langle\varepsilon|\,\Pi\rho_{\text{xuv}}\Pi^{\dagger}\,|\varepsilon\rangle + \langle\varepsilon|\,\Pi^{\dagger}\rho_{\text{xuv}}\Pi\,|\varepsilon\rangle + \mathcal{O}(g_c^4) \tag{110}$$

In this case, we have $\Pi = g_\omega \Pi_\omega$, because we only have one IR pulse, with a square profile in the frequency plane (which is why we don't also have an $\omega + \delta\omega$ term).

Now, consider the contribution from one of the above terms with Π_ω operators. One ends up with

$$\begin{aligned}\langle\varepsilon|\,\Pi_\omega \rho_{xuv}\Pi_\omega^{\dagger}\,|\varepsilon\rangle = \int \mathrm{d}\omega\mathrm{d}\varepsilon'\mathrm{d}\omega'\mathrm{d}\varepsilon''\; & g_\omega g^*_{\omega'}\mu_{\varepsilon'+\omega\,,\varepsilon'}\mu^{*\prime}_{\varepsilon'+\omega\,,\varepsilon'} \\ \times\; & \langle\varepsilon|\varepsilon'+\omega\rangle\,\langle\epsilon'|\,\rho_{xuv}\,|\varepsilon''\rangle\,\langle\varepsilon''+\omega'|\varepsilon''\rangle\,,\end{aligned}$$

where we now have

$$g_\omega = e^{i\omega\tau}(\theta(\omega-\omega_0+\sigma_\omega/2)-\theta(\omega-\omega_0-\sigma_\omega/2)) = e^{i\omega\tau}h_\omega, \tag{111}$$

We rewrite the above by using $\langle\varepsilon|\varepsilon'+\omega\rangle = \delta(\varepsilon'+\omega-\varepsilon) = \delta(\varepsilon'-(\varepsilon-\omega))$ and equivalently for the other braket expression. This gives us the following integral expression:

$$\mathcal{S}_1 = \int \mathrm{d}\omega\mathrm{d}\varepsilon'\mathrm{d}\omega'\; g_\omega g^*_{\omega'}\mu_{\varepsilon'+\omega\,,\varepsilon'}\mu^{*\prime}_{\varepsilon'+\omega\,,\varepsilon'}\delta(\varepsilon'-(\varepsilon-\omega))\,\langle\epsilon'|\,\rho_{xuv}\,|\varepsilon-\omega'\rangle$$

which can be rewritten as

$$\mathcal{S}_1 = \int \mathrm{d}\omega\mathrm{d}\omega'\; g_\omega g^*_{\omega'}\mu_{\varepsilon'+\omega\,,\varepsilon'}\mu^{*\prime}_{\varepsilon'+\omega\,,\varepsilon'}\,\langle\varepsilon-\omega|\,\rho_{xuv}\,|\varepsilon-\omega'\rangle \tag{112}$$

Now, consider the contribution from the other term, and call it $\mathcal{S}_2$, such that we get the complete lowest-order contribution $\mathcal{S} = \mathcal{S}_1 + \mathcal{S}_2$. This second term, i.e.

$$\langle\varepsilon|\,\Pi_\omega^{\dagger}\rho_{xuv}\Pi_\omega\,|\varepsilon\rangle \tag{113}$$

is extremely similar to the one we already saw, in fact it is purely a complex conjugate of the contribution from the other term. As such we can ignore its contribution when simulating the results.

Now, we consider which oscillation frequency we have in expression 112. By considering equation 111, the dependence on the shear frequency can be seen from the following:

$$g_\omega g^*_{\omega'} = e^{i\delta\omega\tau}h_\omega h^*_{\omega'}, \tag{114}$$

where $\delta\omega = \omega - \omega'$. To arrive at the final expression, we Fourier transform the integral expression in equation 112. The important thing to note is

$$\mathcal{F}(e^{i(\omega-\omega')\tau}) \propto \delta(\omega-\omega'-x) \tag{115}$$

Where x is the transform variable, which is a frequency since we transform from the time domain (specified by τ) to the frequency domain (specified by x). We

set x as $\delta\omega$. Also keep in mind that in the simulation we set the μ terms to unity, and for that reason those are excluded from this treatment. The Dirac delta function we get by performing this transform turns equation 112 into the following:

$$S_{\mathcal{F}} \sim \int \mathrm{d}\omega \; h_\omega h^*_{\omega-\delta\omega} \left\langle \epsilon - \omega \right| \rho_{xuv} \left| \varepsilon - (\omega - \delta\omega) \right\rangle, \tag{116}$$

where

$$h^*_{\omega-\delta\omega} = h_{\omega-\delta\omega} = \theta(\omega - \delta\omega - \omega_0 + \sigma_\omega/2) - \theta(\omega - \delta\omega - \omega_0 - \sigma_\omega/2) \tag{117}$$

and x is $\delta\omega$ as previously used. Considering the overlap between the two rectangular pulses we get the following:

$$S_{\mathcal{F}} \sim \int_{\omega_0-\sigma_\omega/2+\delta\omega}^{\omega_0+\sigma_\omega/2} \rho_{xuv}(\varepsilon - \omega + \delta\omega,\ \varepsilon - \omega)\, \mathrm{d}\omega, \tag{118}$$

Here we have used the product of rectangular functions to simply cut off the integration interval. Note the new notation for the integrand. $\rho(a, b)$ here is simply $\langle a| \rho |b\rangle$ written in a more compact form. Taking the gradient of this in the ω direction we get the following:

$$\partial S_{\mathcal{F}} \sim \rho_{xuv}(\varepsilon - \omega_0 - \sigma_\omega/2 + \delta\omega,\ \varepsilon - \omega_0 - \sigma_\omega/2) - \rho_{xuv}(\varepsilon - \omega_0 + \sigma_\omega/2,\ \varepsilon - \omega_0 + \sigma_\omega/2 - \delta\omega). \tag{119}$$

Thus there are two terms which contribute to this gradient. When applying this to data analysis, the goal would be to isolate one of the terms. This is because each of these terms is, individually, a density matrix element (just evaluated for different arguments). The attempts at solving this problem numerically will be outlined in the next section.

8.2.1 Protocol applied to data

What we now want to do is to examine what happens when the above protocol is applied to simulation data. We start by considering the case of an IR bandwidth of 500 nm. This number was somewhat arbitrarily chosen, but the main idea is that the two terms in equation 119 are completely separated. Recall that while bandwidth in question is the IR bandwidth, the two terms of the density matrix correspond to the XUV pulse. So a sufficiently large IR bandwidth corresponds to an essentially complete separation of the two XUV density matrix components.

Now, consider the part of the delay scan from which we acquire the information used in KRAKEN, as in the case of figure 4 b). This part of the scan can be seen in figure 18 below:

As outlined in the theoretical description of the KRAKEN protocol, the above scan is Fourier transformed to extract the desired frequency component, which can be seen in figure 19 below:

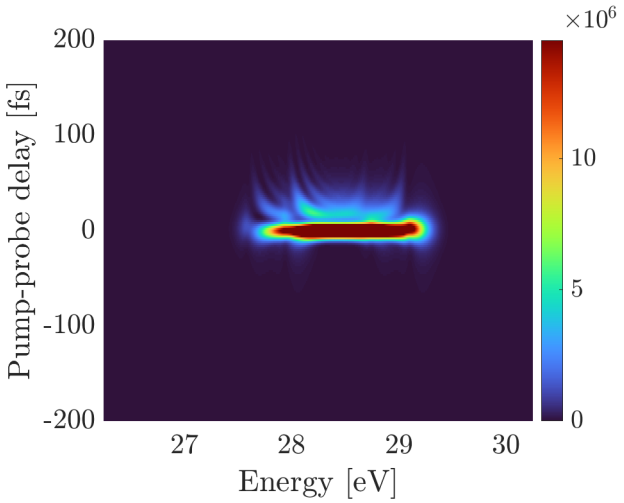

Figure 18: The oscillating part of the scan, which has the pump-probe delay on the vertical axis and energy on the horizontal axis. Equivalent to figure 4 b).

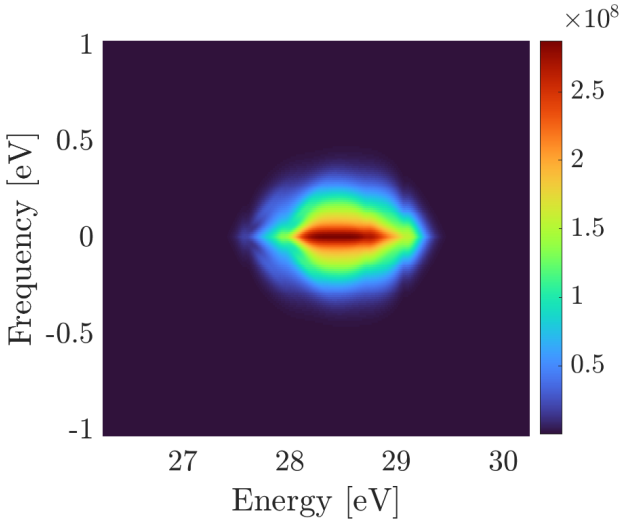

Figure 19: Fourier transform of the scan seen in figure 18.

Now, as outlined in the theoretical description of the square spectrum protocol, we take the gradient of the Fourier transformed scan seen in figure 19 above. Doing this, as predicted one gets two components for which one provides the desired density matrix.

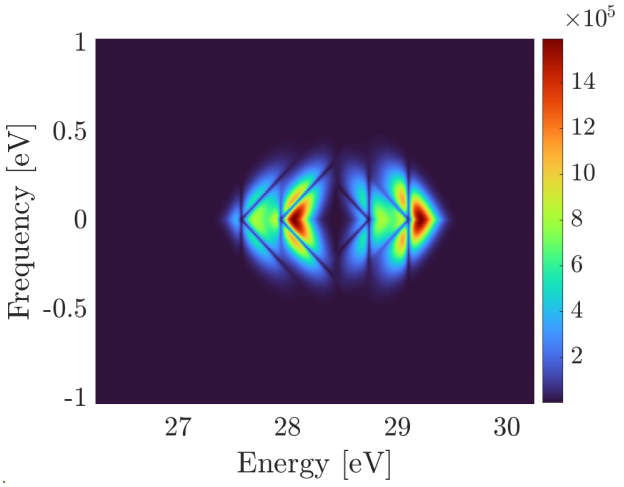

Figure 20: The gradient of the Fourier transform of the spectrum plotted. This matrix is thus equivalent to what we have in equation 119.

In the above figure, we see the plotted equivalent of equation 119, and as expected we see the two terms distinguished clearly with this choice of bandwidth. What we want to do is to focus on just one of these terms, and perform some appropriate Matlab operations to get the axes to match the simulation result used in the original KRAKEN paper [2]. In more specific terms, the circshift function was used to "straighten out" the elements in the left matrix, to align it with the axes in such a way as to match the density matrix discussed in the previous sections. Doing this, we get the following result:

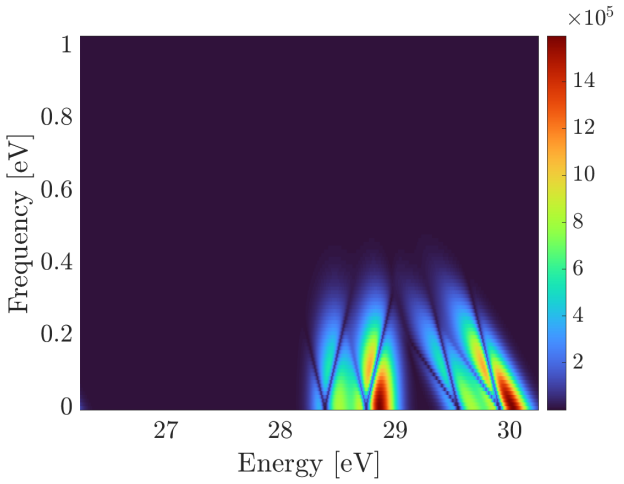

Figure 21: The data in figure 20 reworked so that we see half and have prepared the left side to reconstruct the density matrix (hence the new angles).

Here we have circshifted one of the components to get a result which more closely matches the one we see in the original KRAKEN paper [2]. We can see that the left part is exactly the desired density matrix, except it's only half of it and the scale is slightly off. Dealing with these two things, we end up with the following:

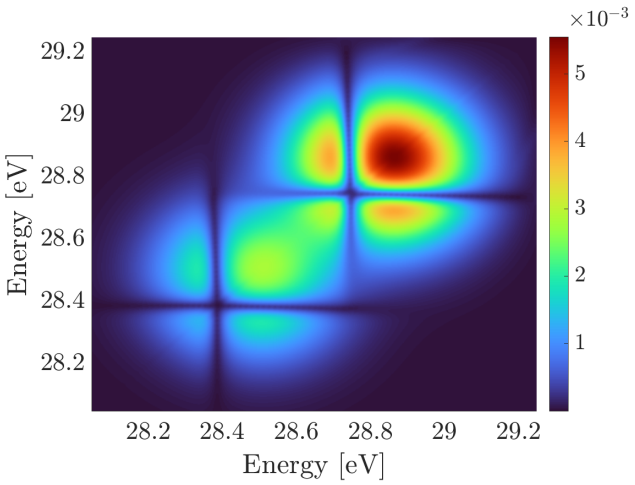

Figure 22: The data in figure 21 treated such that we take the left one of the two contributions and rework the axes such that we recover the density matrix. Note that the result in that figure is now mirrored and conjugated across a diagonal, as should be done to construct a density matrix.

Which we can see is exactly the density matrix that was recovered through quantum state tomography through simulations in the original paper [2]. Now, consider the phase. The phase can be recovered from the interference between the two components that give the coherences.

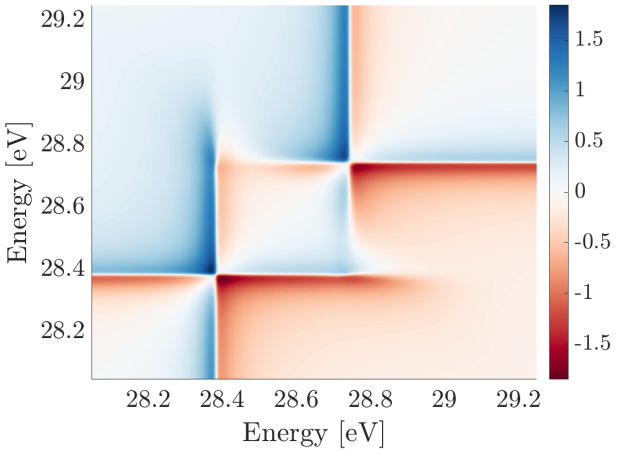

Figure 23: Phase corresponding to the density matrix in figure 22.

The above figure is also very consistent with the results found in the original paper [2]. Now, the above results are for a very ideal case. Having an extremely spectrally broad and flat IR pulse is an ideal case, which is extremely difficult to actually achieve experimentally (and literally not possible with any experimental equipment available for this research). This result is simply an indication that equation 119 is consistent with the same kinds of simulations as the ones used in the KRAKEN paper [2]. So the next step is to study what happens when we actually decrease the IR bandwidth. We start by considering half of the above IR bandwidth, i.e. 250 nm. Since 500 nm gave us more or less complete separation, we expect that when we take 250 nm we have that the two terms in equation 119 overlap such that for each of them, half is isolated from the other, but the remaining half is overlapping with it. Where this overlap occurs, we see a loss of information that we want to work around.

The solution for this case is, in principle, very simple. We can simply choose to take the information from the two isolated halves and combine them into one to reconstruct the above density matrix. Doing this, we end up with the figure below:

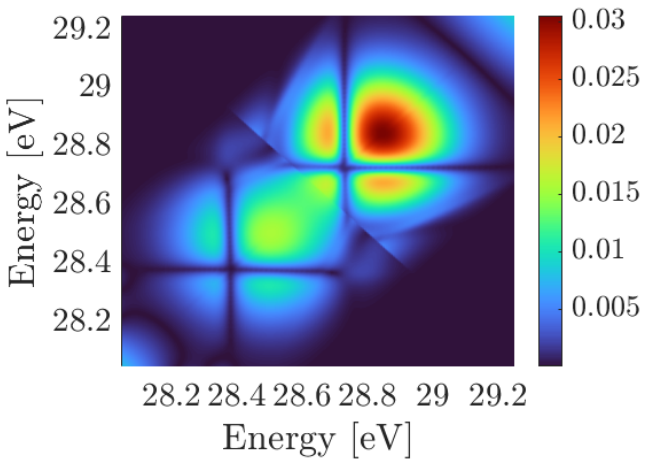

Figure 24: Attempt at reconstructing the density matrix for an IR bandwidth of 250 nm. Notice where the two halves meet, we have a loss of information, as evident by the inconsistency between this result and the one seen in figure 22, not to mention the evident discontinuity which is also inconsistent with the physics at hand.

As can be seen in figure 24, we have recovered essentially the same matrix as the density matrix we are looking for, except a slight loss of information occurring near the middle, where the two halves are "cut off". One can suspect that a further decrease of the IR bandwidth is going to lead to further loss of information until the protocol is no longer usable for analyzing actual experimental data.

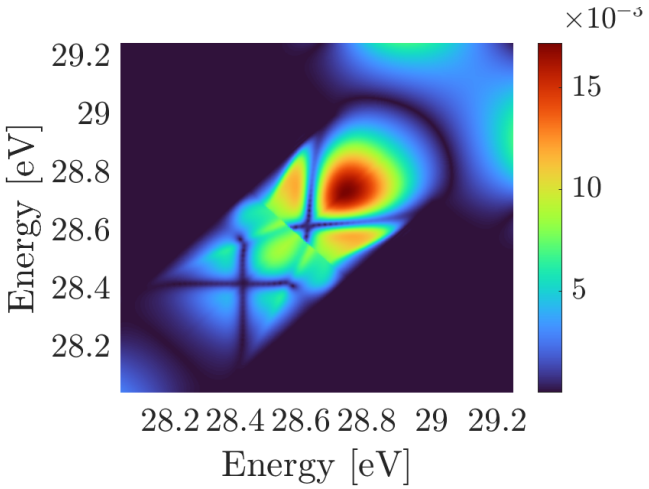

Figure 25: Attempt at reconstructing the density matrix for an IR bandwidth of 125 nm. Notice that the loss of information is quite significant, when compared to figure 22, much more so than in figure 24. At this point, the protocol is no longer robust enough to be usable in experiments.

Indeed, as can be seen in figure 25, the loss of information has become quite significant. Not only is the matrix thinner across the anti-diagonal (representing the main diagonal of the density matrix), but the distortion of the picture around the middle is much more significant. At this stage, as we approach values for bandwidth more similar to the ones used in the lab, the protocol falls apart and is no longer usable for real experiments. This means that while equation 119 seems to be powerful, at least when considering simulation results, there is yet a robust method for using this to actually deal with broadband contributions to experimental data. One should take equation 119 as being the main result of this section, with the simulation result for 500 nm being the indication of its validity. The remaining discussion regarding the shortening of the IR pulse's spectral width is a negative result as is.

8.2.2 Two square pulses

The case considered here is one for which we only have one IR pulse, and where both the single IR pulse and the XUV pulse are square in the frequency domain. By having a large IR bandwidth of 500 nm, we can easily examine the feasibility of the above square pulse protocol.

Direct calculation gives the following density matrix:

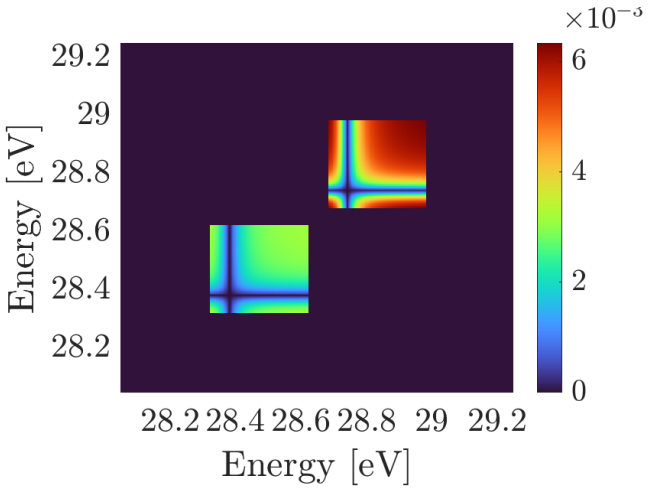

Figure 26: Direct calculation of density matrix for two square pulses, with IR bandwidth 500 nm.

Taking the gradient of the fourier transformed spectrum, as described in the protocol, one gets the following result:

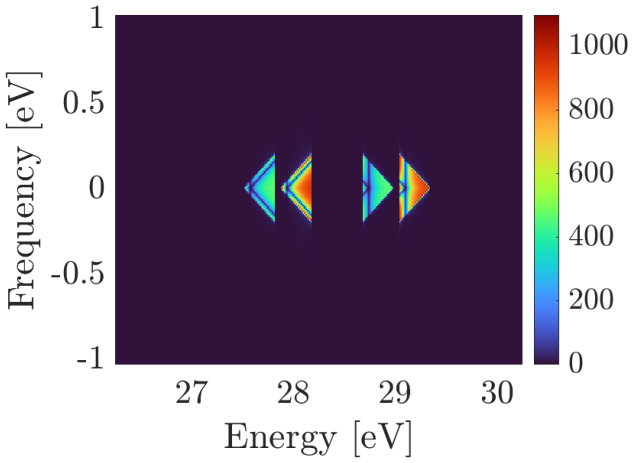

Figure 27: Gradient of the spectrum for two square pulses, with the same pulse parameters as for the direct calculation case.

Comparison with the theoretical protocol tells us that we have two terms and what to isolate one of them. Taking exclusively the left part of the above figure, and rearranging in Matlab, one ends up with the following result:

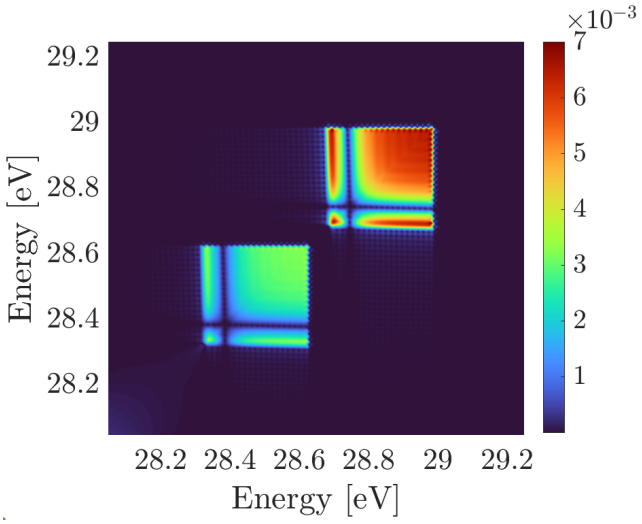

Figure 28: Left side of the gradient of the spectrum, with circshift employed to make the angles closer to the direct calculation case.

As can be seen here, we can acquire the density matrix for this case using this method. The same information is contained here as was seen in figure 26.

9 Summary and conclusions

In this work the proposed KRAKEN protocol has been discussed. This discussion has been separated into roughly two parts. One of them is aimed at explaining the protocol in question, with special attention being given to providing the necessary theoretical background to understanding not only the protocol in principle, but also how it was implemented numerically in simulations.

To this end, we began by describing the principles of the KRAKEN protocol. In short, it is a form of quantum state tomography (QST), which means that it aims to provide a way of reconstructing a density matrix by changing a frequency variable in measurements. Specifically a pump-probe scheme was considered where the probe is a bichromatic IR field. Having the transitions driven by two IR pulses and one XUV pulse respectively, one finds that the Fourier transform with respect to delay (and evaluated at the shear frequency) is proportional to the subdiagonals of the density matrix. This means that varying the shear frequency allows us to reconstruct the density matrix of the photoelectron and thus KRAKEN is a QST protocol.

Special care was taken to motivate a choice of electron wave packet (EWP) to study. The two requirements were that it needed to have an interesting enough structure, and that it needed to exhibit entanglement to justify the use of a QST protocol over, for example, RABBIT. The case study chosen was argon. The structure came from Fano resonances, and the entanglement came from

the spin-orbit splitting of the energy level under consideration. Following that, the amplitude of the density matrix of the EWP in question was studied (from direct calculation).

KRAKEN simulations were then discussed, starting with a theoretical description of two-photon transitions, to show the theory underlying the code. After that, a comparison was made between direct calculation and KRAKEN simulation for the case of an EWP from helium ionization.

The next part of the thesis is a discussion of the limitations and extensions of the KRAKEN protoco. As for limitations, special attention was given to the limitation given by the IR bandwidth, and its effects were demonstrated through simulation.

The extension was focused on overcoming the issue of KRAKEN being experimentally very demanding. The possible solution investigated was a so-called single pulse KRAKEN, for which two variants were suggested. The first was the use of a chirped IR pulse, and the second was the use of a square spectrum IR pulse. Neither of these were fully extended into a functioning KRAKEN simulation.

References

[1] J.B. Altepeter, D.F.V. James, P.G. Kwiat *Quantum State Tomography*, Dept. of Physics, University of Illinois at Urbana-Champaign, Urbana IL. Theoretical Division T-4, Los Alamos National Laboratory, Los Alamos, New Mexico

[2] H. Laurell, D. Finkelstein-Shapiro, C. Dittel et al. *Continuous variable quantum state tomography of photoelectrons* Dept. of physics, Lund University. Atomic physics division.
arXiv link: https://arxiv.org/abs/2202.06798

[3] D. Busto *Quantum interference effects in attosecond photoionization dynamics*, Department of Physics, Lund University, 2020

[4] U. Fano *Effects of Configuration Interaction on Intensities and Phase Shifts*, Washington Bureau of Standards, Washington, D.C., 1961, Vol. 124, Iss. 6

[5] M. Turconi et al. *Spin-orbit-resolved spectral phase measurements around a Fano resonance*, Journal of Physics B: Atomic, Molecular and Optical Physics 53, 184003, 2020

[6] Á. Jímenez-Galán, F. Martín, L. Argenti *Two-photon finite-pulse model for resonant transitions in attosecond experiments*, Physical Review A, 2016, Vol. 93

[7] D. Busto *Spin-orbit resolved two-photon transition amplitudes via the* $3s^{-1}4p$ *Fano resonance in argon*, Supplementary material to KRAKEN paper, November 2021

[8] L. Argenti *Extension of the two-photon finite-pulse model to include spin-orbit coupling in Ar: Field-free and dipolar couplings between the essential resonances and channels*, Supplementary material to [6], February 2020

[9] M. Turconi et al. *Spin-orbit-resolved spectral phase measurements around a Fano resonance*, J. Phys. B: At, Mol. Opt. Phys. 53 184003, 2020

[10] B.E.A. Saleh, M.C. Tiech, *Fundamentals of Photonics*, 1991, Wiley, New York (NY)

[11] Wikimedia Commons, https://commons.wikimedia.org/wiki/File:Fano-resonance-scs.png